The Role of Type I Interferon in Regulating Macrophage Responses to *Salmonella* Typhimurium Infection

Inaugural Dissertation

zur

Erlangung des Doktorgrades
Dr. nat. med.

der Medizinischen Fakultät
und
der Mathematisch-Naturwissenschaftlichen Fakultät
der Universität zu Köln

vorgelegt von

Nina Judith Hos

aus Nürnberg

Hundt Druck, Köln

2019

STATEMENT

Parts of this work, including Material and Methods, Results, and Discussion section, have been published previously in the *Journal of Cell Biology* with the title "*Type I interferon enhances necroptosis of Salmonella Typhimurium-infected macrophages by impairing anti-oxidative stress responses.*" (Hos NJ, Ganesan R, Gutierrez S, Hos D, Klimek J, Abdullah Z, Krönke M, Robinson N. 2017; 216(12):4107-4121. doi: 10.1083/jcb.201701107).

TABLE OF CONTENTS

SUMMARY

Salmonella Typhimurium (*S.* Typhimurium) is a Gram-negative, facultative intracellular bacterium that exploits the host's type I interferon (IFN-I) response to induce cell death in macrophages. We have previously demonstrated that activation of the IFN-I receptor (Ifnar1) results in recruitment of RIP1 and subsequent formation of a RIP1/RIP3 complex, leading to a specific form of programmed cell death, termed necroptosis, in *S.* Typhimurium-infected macrophages (Robinson et al. 2012). Despite our detailed knowledge on IFN-I/RIP1/RIP3-dependent necroptosis execution, the IFN-I-mediated pathways that determine whether infected macrophages will undergo necroptosis remain elusive. This work therefore sought to identify the IFN-I-mediated events that sensitize *S.* Typhimurium-infected macrophages to cell death.

Here, we demonstrate that *S.* Typhimurium infection causes mitochondrial damage and impairs the host´s anti-oxidative stress response through upregulation of the mitochondrial phosphatase Pgam5 downstream of IFN-I/RIP3. Pgam5 subsequently interacts with the transcription factor Nrf2, which sequesters Nrf2 in the cytosol thereby repressing the transcription of Nrf2-dependent anti-oxidative genes. The impaired ability to respond to *S.* Typhimurium-induced oxidative stress results in ROS-mediated mitochondrial damage, ATP depletion, transient induction of autophagy, and autophagy-mediated degradation of p62, which impairs p62-Keap1 interaction. Consequently, Keap1 interacts more with Nrf2, which further represses Nrf2 function and additionally impairs anti-oxidative stress responses to *S.* Typhimurium infection thereby sensitizing macrophages to cell death.

Taken together, we identify impaired Nrf2-dependent redox homeostasis of *S.* Typhimurium-infected macrophages as an important mechanism that drives cell death downstream of IFN-I/RIP3.

ZUSAMMENFASSUNG

Salmonella Typhimurium (*S.* Typhimurium) ist ein Gram-negatives, fakultativ intrazelluläres Bakterium, welches die Typ-I-Interferon (IFN-I)-Antwort des Wirts ausnutzt, um den Zelltod in Makrophagen zu induzieren. Unsere Vorarbeiten zeigen, dass die Aktivierung des IFN-I-Rezeptors (Ifnar1) zur Rekrutierung von RIP1 und zur anschließenden Bildung eines RIP1/RIP3-Komplexes führt, was zu einer bestimmten Form des programmierten Zelltods, der sogenannten Nekroptose, in mit *S.* Typhimurium infizierten Makrophagen führt (Robinson et al. 2012). Trotz unseres detaillierten Wissens über die Mechanismen der IFN-I/RIP1/RIP3-abhängigen Nekroptose sind die durch IFN-I vermittelten Signalwege, die darüber bestimmen, ob infizierte Makrophagen ihr Nekroptose Programm ausführen, weiterhin unklar. Ziel dieser Arbeit ist es daher, die durch IFN-I vermittelten Ereignisse zu identifizieren, die mit *S.* Typhimurium infizierte Makrophagen für den Zelltod sensibilisieren.

Unsere Ergebnisse zeigen, dass die Infektion mit *S.* Typhimurium eine Schädigung der Mitochondrien verursacht und die anti-oxidative Stressreaktion des Wirts beeinträchtigt, indem die mitochondriale Phosphatase Pgam5, welche IFN-I/RIP3 nachgeschaltet ist, hochreguliert wird. Pgam5 interagiert anschließend mit dem Transkriptionsfaktor Nrf2, wodurch Nrf2 im Cytosol sequestriert und die Transkription von Nrf2-abhängigen anti-oxidativen Genen beeinträchtigt wird. Die eingeschränkte Fähigkeit auf *S.* Typhimurium-induzierten oxidativen Stress zu reagieren, führt zur ROS-vermittelten Schädigung von Mitochondrien, einem ATP Mangel, der vorübergehenden Induktion von Autophagie und der autophagievermittelten Degradation von p62, welches die p62-Keap1-Interaktion beeinträchtigt. Folglich interagiert Keap1 vermehrt mit Nrf2, wodurch die Funktion von Nrf2 weiter eingeschränkt wird und die anti-oxidative Stressantwort gegen *S.* Typhimurium zusätzlich beeinträchtigt wird, wodurch Makrophagen für den Zelltod sensibilisiert werden.

Zusammenfassend haben wir die gestörte Nrf2-abhängige Redox-Homöostase als einen wichtigen Mechanismus identifiziert, der den Zelltod von mit *S.* Typhimurium infizierten Makrophagen stromabwärts von IFN-I/RIP3 vermittelt.

ABBREVIATIONS

AREs	Antioxidant response elements
Atg7^{-/-}	Autophagy-related protein 7 deficient macrophages
ATP	Adenosine triphosphate
BMDMs	Bone marrow-derived macrophages
CFUs	Colony forming units
ConcA	Concanamycin A
Ctrl	Control
Drp1	Dynamin-related protein 1
Gapdh	Glyceraldehyde 3-phosphate dehydrogenase
Gclc	Glutathione synthesis enzyme glutamate cysteine ligase
Hmox-1	Heme oxygenase-1
IFN-I	Type I interferon
IFN-β	Interferon beta
Ifnar1^{-/-}	Type I interferon receptor deficient macrophages
IgG	Immunoglobulin G
Keap1	Kelch-like ECH-associated protein 1
LC3	Microtubule-associated proteins 1A/1B light chain 3B
LDH	Lactate dehydrogenase
LPS	Lipopolysaccharide
MFI	Mean fluorescence intensity
MLKL	Mixed lineage kinase domain-like protein
MOI	Multiplicity of infection
mRNA	Messenger RNA
mTORC1	Mechanistic target of rapamycin complex 1
mtROS	Mitochondrial reactive oxygen species
Ψm	Mitochondrial membrane potential
Nqo1	NAD(P)H quinone oxidoreductase 1
Nrf2	Nuclear factor (erythroid-derived 2)-like 2
OCR	Oxygen consumption rate
Pgam5	Phosphoglycerate mutases family member 5
p.i.	Post infection
RIP3	Receptor-interacting protein kinase 3
RIP3^{-/-}	Receptor-interacting protein kinase 3 deficient macrophages

ROS	Reactive oxygen species
S.	*Salmonella*
SCV	*Salmonella* containing vacuole
SD	Standard deviation
SPI	*Salmonella* pathogenicity island
Sqstm1/p62	Sequestosome-1
ST	*Salmonella* Typhimurium
S6K	S6 kinase
TLR	Toll like receptor
TMRM	Tetramethylrhodamine methyl ester
TNF	Tumor necrosis factor
Tom20	Translocase of outer membrane subunit 20
T3SS	Type 3 secretion system
UI	Uninfected
WT	Wildtype

1.   Introduction

1.1   *Salmonella* Typhimurium infection

1.1.1   Microbiology and epidemiology of *S.* Typhimurium

Salmonellae are Gram-negative, rodshaped bacteria that infect or colonize a wide range of mammalian hosts worldwide. *Salmonellae* are motile, facultative intracellular and facultative anaerobe bacteria that belong to the large family of Enterobacteriaceae. The genus *Salmonella* consists of two species, *Salmonella enterica* and *Salmonella bongori*. *Salmonella enterica* is further divided into six different subspecies. In total, about 2,500 different *Salmonella* serotypes have been identified with most of the clinically relevant serotypes belonging to subspecies I (*Salmonella enterica*, subspecies enterica) (Tindall et al. 2005).

Humans infected with *Salmonella* typically present with symptoms of gastroenteritis or typhoid fever (systemic infection with fever and abdominal symptoms). Gastroenteritis can be caused by numerous different *Salmonella* serotypes (~ 500 serotypes) that are collectively known as nontyphoidal *Salmonellae* (NTS), whereas typhoid fever is predominantly caused by *Salmonella enterica* serovar Typhi and Paratyphi (Robert Koch Institute 2019). The global burden of NTS gastroenteritis has been estimated at about 94 million cases and 155,000 deaths per year (Majowicz et al. 2010). In Germany, more than 12,000 cases of NTS were reported in 2018 according to the Robert Koch Institute (Robert Koch Institute 2019). Children below the age of five years, elderly people and patients with immunosuppression are more susceptible to *Salmonella* infection (Ryan and Ray 2004). Among NTS, *Salmonella enterica* serovar Enteritidis (*S.* Enteritidis) and *Salmonella enterica* serovar Typhimurium (*S.* Typhimurium) are of particular interest, as they are the most commonly isolated serotypes worldwide (Lan et al. 2009; World Health Organisation 2019).

1.1.2   Pathogenesis of *S.* Typhimurium

S. Typhimurium infection is usually acquired by oral ingesting of contaminated food, such as dairy products, eggs or meat. Approximately 10^4 to 10^6 bacteria are sufficient to cause infection in humans (Robert Koch Institute 2019). After overcoming gastric acidity, *S.* Typhimurium penetrates the epithelial barrier of the small intestine (**Fig. 1**). It actively invades intestinal epithelial cells or it induces its phagocytic uptake by microfold cells (M cells) that overlie the lymphoid follicles of Peyer's patches (Jones et al. 1994). In humans, *S.* Typhimurium infection usually does not proceed beyond the lamina propria. In mice and immunocompromised patients, however, *S.* Typhimurium gains access to the basolateral side of the intestine, where it is sensed and phagocytosed by monocytic-derived cells of the gut-associated lymphatic tissue (GALT), predominantly macrophages and dendritic cells (Broz et al. 2012). In susceptible hosts, *S.* Typhimurium enters the lymphatic system and the bloodstream via infected monocytes, allowing *S.* Typhimurium to spread to the liver and the spleen thereby establishing systemic infection (Vazquez-Torres et al. 1999).
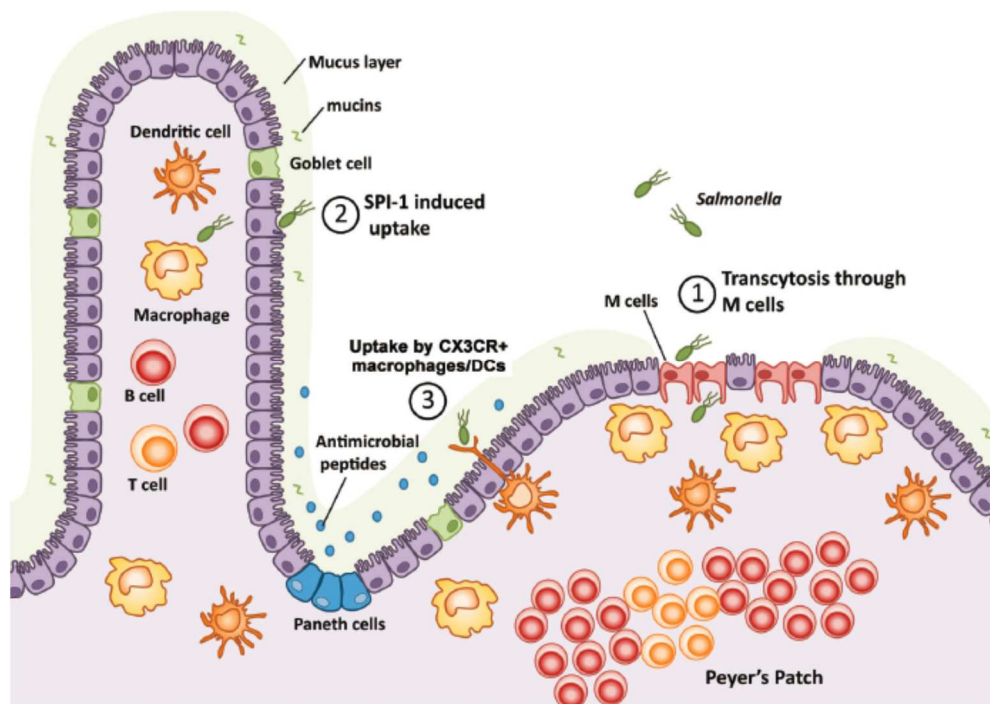
Figure 1. Schematic representation of *S.* Typhimurium invading the intestinal mucosa.

(1) The major route of *Salmonella* invasion is via transcytosis through M cells at the Peyer´s Patches followed by **(2)** *Salmonella* pathogenicity island 1 (SPI-1)-mediated invasion of enterocytes. Alternatively, **(3)** *Salmonella* can

Following epithelial cell invasion or phagocytic uptake, *S.* Typhimurium is engulfed in a membrane-derived compartment called *Salmonella*-containing vacuole (SCV) (Bakowski et al. 2008). In a strict sense, SCVs are only formed in epithelial cells, whereas in professional phagocytes *S.* Typhimurium is taken up by phagosomes. SCVs show certain characteristics of late stage endosomes and express lysosomal markers that include lysosome-associated membrane proteins (LAMPs), the GTPase Rab7 and vacuolar ATPases (LaRock et al. 2015). However, further maturation of the SCV does not occur as *S.* Typhimurium actively inhibits SCV fusion with the lysosome thereby preventing its enzymatic degradation (LaRock et al. 2015). The ability of *S.* Typhimurium to persist in host cells, including macrophages, is crucial for its pathogenesis, as strains lacking this ability are non-virulent (Bakowski et al. 2008).

S. Typhimurium virulence is highly dependent on the expression of two distinct type III secretion systems (T3SSs) and several effector proteins that are encoded on large chromosomal clusters termed *Salmonella* pathogenicity island 1 (SPI-1) and SPI-2. The T3SS apparatus, which is highly conserved among Gram-negative bacteria, forms a needle-like complex that mediates the injection of bacterial translocon and effector proteins into the host cell`s cytoplasm (Aizawa 2001). SPI-1-encoded T3SS effector proteins, such as SipA, SopB and SopE, are essential for epithelial invasion by inducing actin cytoskeleton rearrangements leading to membrane ruffling and subsequent uptake of *S.* Typhimurium (LaRock et al. 2015). A major function of the SPI-2-encoded T3SS effector proteins, such as SifA and SsrB, is the modification of the SCV to enable intracellular survival and replication of *S.* Typhimurium within the inhospitable milieu of the SCV (Hensel et al. 1998).

1.2 Interaction of *S.* Typhimurium with macrophages

1.2.1 Activation of inflammatory pathways

Once *S.* Typhimurium has passed the epithelial barrier of the small intestine, it is targeted by cells of the innate immune system, predominantly macrophages. Macrophages

sense *S.* Typhimurium through their pattern recognition receptors (PRRs), which mediate recognition of pathogen-associated molecular pattern molecules (PAMPs). Toll-like receptors (TLRs) function as the PRRs in mammals and play a major role in the defense against extracellular and intracellular *S.* Typhimurium. TLRs can be activated by a variety of *S.* Typhimurium-derived ligands, such as peptidoglycan and lipoproteins (TLR2), LPS (TLR4), flagellin (TLR5) and CpG-rich repeats of bacterial DNA (TLR9) (Broz et al. 2012). TLR activation engages the signaling adaptors MyD88 and TRIF that culminate in the activation of nuclear factor- κB (NF-κB) and interferon regulatory factor 3 (IRF3), which control the expression of several pro-inflammatory cytokines as well as type I interferon (IFN-I) (Medzhitov 2001). The induction of inflammatory signaling pathways is necessary for the generation of a robust antimicrobial milieu and for the proper activation of adaptive immune responses.

1.2.2 Induction of oxidative stress

Reactive oxygen species (ROS) are essential components of the innate immune response against invading pathogens. Upon *S.* Typhimurium infection, ROS contribute to the efficient control of intracellular *S.* Typhimurium, as ROS increases the phagosomal bactericidal activity of macrophages (West et al. 2011). Macrophages have been shown to generate ROS through the phagosomal NADPH oxidase and the mitochondrial oxidative phosphorylation (OXPHOS) machinery (Lambeth 2004). ROS comprises oxygen free radicals, such as superoxide anion radical ($O_2^{\cdot-}$) and hydroxyl radical ($^{\cdot}OH$), and non-radical oxidants, such as hydrogen peroxide (H_2O_2) and singlet oxygen ($^1O_2$), which can be interconverted from one to another (Zorov et al. 2014). The majority of mitochondrial ROS (mtROS) are derived from complex I or complex III of the electron transport chain (Murphy 2009). Although mtROS have been recognized as important signaling hubs linking mitochondrial to cytoplasmic signals, extensive mtROS production results in oxidative DNA damage and cell death (Murphy 2009). Therefore, mtROS levels have to be tightly controlled by a versatile antioxidant system.

Nuclear factor-erythroid 2-related factor 2 (Nrf2) is a key transcription factor that neutralizes cellular ROS by inducing multiple genes whose products have anti-oxidative functions. Kelch-like ECH-associated protein 1 (Keap1), a redox regulated substrate adaptor for a cullin-based ubiquitin ligase, is the major negative regulator of Nrf2 (Lo and Hannink 2008). Under resting conditions, Keap1 sequesters Nrf2 in the cytoplasm and mediates Nrf2 ubiquitination and its subsequent degradation via the proteasomal pathway (Kobayashi et al. 2004; Zhang et al. 2004). In response to oxidative stress, however, Nrf2 is released from Keap1 and translocated into the nucleus, where it binds to conserved antioxidant response elements (AREs) in the promoter regions of target genes, such as the detoxification enzyme NAD(P)H quinone oxidoreductase 1 (*Nqo1*), glutathione synthesis enzyme glutamate cysteine ligase (catalytic subunit, *Gclc*), and cell stress protein heme oxygenase-1 (*Hmox-1*) (Ishii et al. 2002; Rushmore et al. 1991; Wasserman and Fahl 1997).

Nrf2 function is negatively regulated by the mitochondrial phosphatase Pgam5, which has originally been identified as a protein bound to Keap1 (Lo and Hannink 2006). Pgam5 contains an N-terminal mitochondrial-localization sequence that mediates its recruitment to the outer mitochondrial membrane, where Pgam5 forms a ternary complex with Keap1 and Nrf2, in which the dimeric Keap1 simultaneously binds Pgam5 and Nrf2 (Lo and Hannink 2008). Nrf2 is consequently sequestered in this inhibitory complex leading to impaired activation of Nrf2-dependent anti-oxidative genes.

Recent studies suggest that the autophagy adaptor protein Sqstm1/p62 (hereafter, p62), is a positive regulator of the Nrf2 pathway. Upon oxidative stress, p62 directly interacts with the Nrf2-binding site of Keap1. Consequently, Nrf2 is released from Keap1 and translocated to the nucleus leading to the transcription of Nrf2-dependent anti-oxidative enzymes (Ichimura et al. 2013; Komatsu et al. 2010; Lau et al. 2010).

1.2.3 Interference with autophagy

Autophagy is a highly-conserved catabolic process that involves the complex interplay of more than 35 autophagy-related proteins (Atgs) allowing the enzymatic degradation of

large intracellular components, such as protein aggregates and long-lived or damaged organelles. Autophagy is usually induced by nutrient starvation through the inhibition of mammalian target of rapamycin complex 1 (mTORC1) leading to the engulfment of endogenous cargo into double-membrane vesicles called "autophagosomes", which are subsequently degraded by the lysosomal pathway (Deretic et al. 2013; Mizushima et al. 2008).

Furthermore, autophagy is known to mediate the degradation of ubiquitinated cargo, such as misfolded proteins and protein complexes. Autophagy of ubiquitinated proteins requires the adaptor protein p62, which contains multiple protein-protein interaction sites, including a C-terminal ubiquitin-associated (UBA) domain and a LC3 interaction region (LIR). These domains allow p62 to bind simultaneously to ubiquitinated cargo and LC3 thereby targeting proteins and organelles for autophagosomal degradation (Bjorkoy et al. 2005; Itakura and Mizushima 2011; Pankiv et al. 2007). Beyond its importance for maintaining cellular energy and protein homeostasis, autophagy has also been shown to have more diverse functions, such as selective removal of proteins or clearance of intracellular pathogens (Sumpter and Levine 2010).

Selective autophagy of invading pathogens (xenophagy) has been recognized as an important component of cell-autonomous immunity. While several studies underscore the importance of xenophagy during infection with *Mycobacterim tuberculosis*, *Listeria monocytogenes*, *Shigella* spp., and *S*. Typhimurium (Cemma and Brumell 2012), the exact mechanism by which intracellular bacteria are recognized by the autophagic machinery remain poorly understood. It has been suggested that approximately 25% of intracellular *S*. Typhimurium escape from the SCV following infection of HeLa cells (Birmingham et al. 2006). Once in the cytosol, *S*. Typhimurium becomes coated with ubiquitin and associates with p62 and other adaptor proteins, such as nuclear dot protein 52 (NDP52), which mediate the LC3-dependent autophagic degradation of *S*. Typhimurium (Levine et al. 2011; Zheng et al. 2009). By contrast to epithelial cells, our recent work has demonstrated that xenophagy is

of minor relevance during *S*. Typhimurium infection of macrophages. While *S*. Typhimurium initially co-localizes with LC3-positive structures, it escapes from these structures during the further course of infection (Ganesan et al. 2017), indicating that it manipulates autophagy.

Probably more important than targeting intracellular bacteria for autophagic degradation, is the interplay between autophagy and innate immune signaling pathways. Indeed, there is increasing evidence that engagement of TLR4 by LPS in macrophages induces autophagy through interaction of TRIF and MyD88 with the autophagy protein beclin-1 (Shi and Kehrl 2008; Travassos et al. 2010). Furthermore, autophagy has been shown to fine-tune innate immune responses through modulation of IFN-I production and inflammasome activation (Sumpter and Levine 2010) as well as mediating cell death (Fitzwalter and Thorburn 2015).

1.2.4 Induction of cell death

For many years, apoptosis has been implicated as the major form of programmed cell death, whereas necrosis has mainly been considered as an accidental cell death process that occurs in response to different pathophysiological stimuli (Vanden Berghe et al. 2014). However, recent genetic evidence and the discovery of specific pharmacological inhibitors of necrosis have redefined necrosis as a highly regulated form of programmed cell death. Necrosis includes many different cell death modalities, such as necroptosis, ferroptosis, pyroptosis, and cell death associated with the release of (neutrophil) extracellular traps, called NETosis or ETosis (Pasparakis and Vandenabeele 2015).

Among these, necroptosis is probably the most extensively studied form of necrosis. Necroptosis is a form of programmed cell death dependent on receptor-interacting Ser/Thr protein kinase (RIP) 1, RIP3 and its substrate mixed lineage kinase like (MLKL). Although many inflammatory signals, including TLR4 and IFN-I receptor activation as well as FAS/TRAIL signaling (Pasparakis and Vandenabeele 2015), can activate necroptotic pathways, the induction of necroptosis has been best exemplified by tumor necrosis factor

receptor (TNFR)-mediated signaling. Engagement of the TNFR induces the formation of a complex containing RIP1, RIP3, TNFR-associated death domain (TRADD), caspase-8, and FAS-associated protein with a death domain (FADD). While activation of caspase-8 results in apoptosis, inhibition of caspase-8, for instance by bacterial or viral proteins, triggers the formation of the necrosome. Autophosphorylation of RIP1 and RIP3 recruits the pseudokinase MLKL, which is itself phosphorylated by RIP3 leading to membrane permeabilization and subsequent cell death (Declercq et al. 2009).

Despite our detailed knowledge on TNF-mediated necroptosis execution, the events pre-ceding necrosome formation remain less understood. Mitochondria have been recognized as important mediators of several cell death modalities (Galluzzi et al. 2012) and ATP depletion by mitochondrial damage has been shown to be a trigger for necrosis (Vanlangenakker et al. 2008). In response to infection, mitochondria can change from a source of energy into organelles that promote cell death by releasing mtROS and toxic proteins that are usually retained within the mitochondrial intermembrane space (Kroemer et al. 2007). Furthermore, the mitochondrial phosphatase Pgam5 has recently been implicated to mediate TNF-induced necroptosis. Mechanistically, Pgam5 is recruited to RIP1- and RIP3-containing protein complexes at the outer mitochondrial membrane, where Pgam5 induces Drp1-mediated mitochondrial fragmentation resulting in necroptotic cell death (Wang et al. 2012).

The induction of cell death is a crucial virulence strategy employed by *S.* Typhimurium (Lindgren et al. 1996). Following invasion of host cells, *S.* Typhimurium requires the temporary niche of the SCV for intracellular adaption and replication, while at later stages of infection *S.* Typhimurium induces cell death to escape from the host cell and to infect surrounding cells. In macrophages, *S.* Typhimurium was found to induce different cell death modalities, including apoptosis-like cell death requiring caspase-8 activation (Lindgren et al. 1996), caspase-1/caspase-11-dependent pyroptosis resulting in IL-1β secretion (Brennan and Cookson 2000), and RIP3 and MLKL-dependent necroptosis via activation of IFN-I signaling pathways (Robinson et al. 2012).

12

1.3 Type I interferon (IFN-I)-dependent immune responses to *S.* Typhimurium

1.3.1 Induction of IFN-I synthesis

IFN-I are immunomodulatory cytokines that are secreted by various mammalian cell types in response to viral and bacterial infection. The family of IFN-I consists of about 20 members, with IFN-α and IFN-β being the major IFN-I expressed upon infection (Bogdan et al. 2004). Most of our knowledge on IFN-I signaling is derived from viral infection, but recent studies have also highlighted the importance of IFN-I for the cell-autonomous defense against bacterial infection (Bogdan et al. 2004).

Following infection, IFN-I synthesis is predominantly induced through activation of the stimulator of interferon genes (STING) pathway. Pathogen-derived DNA is sensed in the cytosol by cyclic GMP–AMP synthase (cGAS), which induces the cyclic dinucleotide (CDN) second messenger cGAMP (cyclic GMP-AMP) to activate the signaling adaptor STING. STING together with TANK-binding kinase 1 (TBK1) is translocated to the perinuclear region, where TBK1 phosphorylates the transcription factor interferon regulatory factor 3 (IRF3). Subsequently, IRF3 translocates to the nucleus and induces the transcription of numerous innate immune genes, including *IFN-β,* the main IFN-I in mice (Barber 2015).

Several bacteria have been shown to activate the STING pathway, such as *Legionella pneumophila, Francisella tularensis, Streptococcus pyogenes, Brucella abortus and Mycobacterium tuberculosis* (Barber 2015; Marinho et al. 2017). STING activation by *S.* Typhimurium, however, has not been reported to date (Marinho et al. 2017) and IFN-I production by *S.* Typhimurium is mainly thought to be mediated through LPS-mediated TLR4 activation (Owen et al. 2016; Sing et al. 2000).Gram-negative infection or binding of LPS to TLR4 engages TIR-domain containing adaptor protein inducing IFN-β (TRIF) and TRIF-related adaptor molecule (TRAM) (Yamamoto et al. 2003). This mediates activation of tank-binding kinase 1 (TBK1) and the inhibitor of nuclear factor-κB kinase (IKK-i), which leads to dimerization and nuclear translocation of IRF3 resulting in the transcription of *IFN-β* and auto- and paracrine signal transduction through the IFN-I receptor (Decker et al. 2005).

1.3.2 Activation of the IFN-I receptor pathway

IFN-I binds to a heterodimeric transmembrane receptor consisting of two subunits, IFN-I receptor (Ifnar) 1 and Ifnar2, respectively (Platanias 2005). Canonical Ifnar activation engages the receptor-associated protein tyrosine kinases Janus kinase 1 (JAK1) and tyrosine kinase 2 (TYK2), which phosphorylate the cytoplasmic transcription factors signal transducer and activator of transcription 1 (STAT1) and STAT2 (Stark and Darnell 2012). After dimerization and nuclear translocation, STAT1 and STAT2 form a complex with IRF9, which is termed IFN-stimulated gene factor 3 (ISGF3). ISGF3 subsequently binds to DNA sequences called IFN-stimulated response elements (ISREs), leading to the transcription of several hundred IFN-I stimulated genes (ISGs), which initiate antimicrobial pathways that limit the spread of infectious agents (Gough et al. 2012).

1.3.3 IFN-I-mediated cell death

Heterologous activation of the IFN-I pathways by various bacterial stimuli results in paradoxical infection outcomes, e.g. the production of IFN-I protects against some intracellular pathogens, such as *Mycobacterium tuberculosis* (Desvignes et al. 2012), while it enhances the susceptibility to other intracellular pathogens, such as *Listeria monocytogenes* (O'Connell et al. 2004).

We have previously demonstrated that *S.* Typhimurium exploits the host´s IFN-I response to induce cell death within macrophages. Activation of the Ifnar1 lead to the recruitment of RIP1, promoting the formation of a RIP1-RIP3 complex, which mediated necroptosis of infected macrophages (Robinson et al. 2012). As a result, mice lacking the Ifnar1 (*Ifnar1*$^{-/-}$) survived significantly better (~30 to 60 days), whereas wildtype (WT) mice died within seven days after *S.* Typhimurium infection (**Fig. 2**).
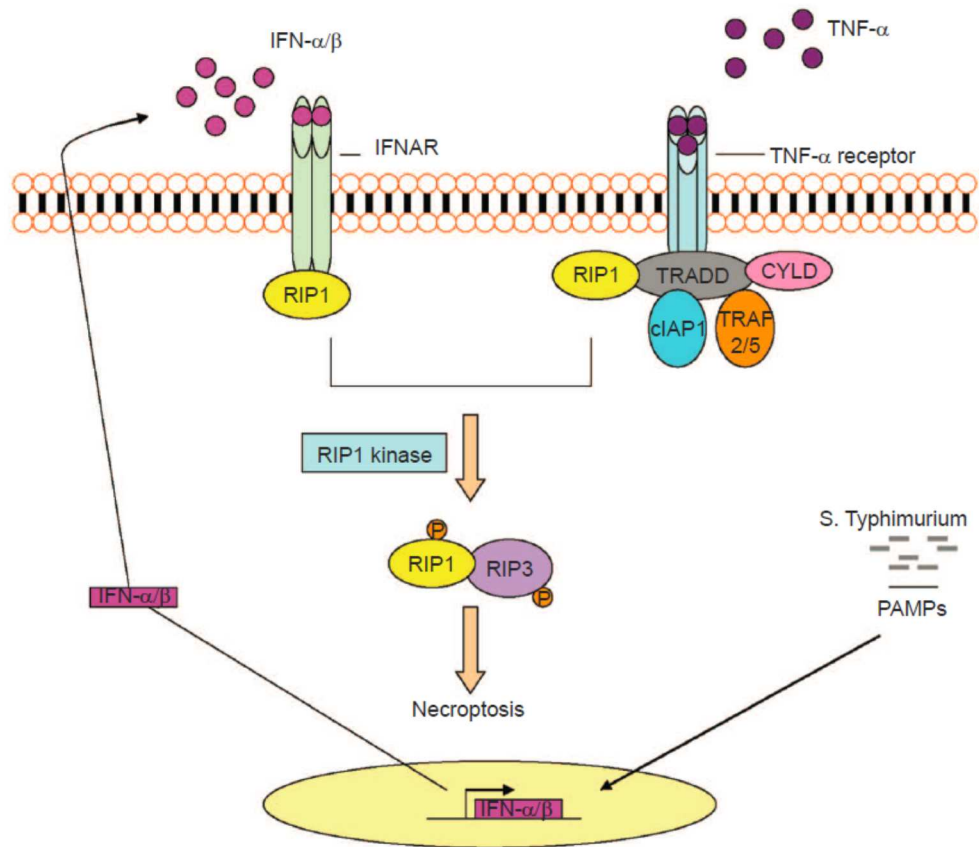
Figure 2. IFN-I-mediated necroptosis in *S*. Typhimurium-infected macrophages.

Following infection of macrophages, *S*. Typhimurium induces TLR4-mediated transcription of *IFN-I* (predominantly *IFN-β*). IFN-I binds to its cognate receptor (IFNAR) in an autocrine manner. RIP1 is subsequently engaged to the IFNAR resulting in the formation of a RIP1/RIP3 containing complex that triggers necroptosis of infected macrophages. In bone marrow-derived macrophages, IFNAR signaling is required for TNF-mediated necroptosis. Figure taken from (Du et al. 2013).

Importantly, better control of *S*. Typhimurium and enhanced survival of *Ifnar1*$^{-/-}$ mice was specifically mediated by macrophages, because macrophages of *Ifnar1*$^{-/-}$ mice increased survival when transferred into WT hosts (Robinson et al. 2012).

HYPOTHESIS

Although our previous work has identified IFN-I-mediated activation of RIP1/RIP3 by *S.* Typhimurium as a novel pathway leading to necroptosis of macrophages, the mechanisms prior to necrosome formation largely remain unknown. We hypothesize that *S.* Typhimurium infection likely induces the same damage in WT and *Ifnar1*$^{-/-}$ macrophages. However, IFN-I signaling impairs the response to *S.* Typhimurium-induced damage in WT macrophages and the inability of WT macrophages to balance cellular homeostasis probably results in necroptosis execution. This work therefore aims to determine the harmful events mediated by IFN-I signaling that precede *S.* Typhimurium-induced cell death of macrophages.

OBJECTIVES OF THIS WORK

1. To determine the role of IFN-I signaling upon *S.* Typhimurium infection of macrophages.

2. To unravel the harmful events mediated by IFN-I signaling leading to cell death of *S.* Typhimurium-infected macrophages.

3. To identify the IFN-I-dependent pathways resulting in cell death of *S.* Typhimurium-infected macrophages.

2. Materials and Methods

2.1 Materials

2.1.1 List of instrumentation

Instrumentation	Company
Countess II cell counter	life technologies
Curix60 developing machine	Agfa
EM109 electron microscope	Zeiss
Enspire multimode plate reader	PerkinElmer
FACSCanto flow cytometer	BD Biosciences
IX81 inverted confocal microscope	Olympus
PCR Cycler CFX96	Bio-Rad
Seahorse XF-96 analyzer	Agilent

2.1.2 List of software

Software	Company
FLOWJO v10.1	Tree Star
Fluoview FV10-ASW v4.2	Olympus
ImageJ	NIH
Primer3web v4.1.0	ELIXIR
Prism v5	GraphPad

2.1.3 List of chemicals and reagents

Chemicals and reagents	Company	Cat. Number
A/G agarose magnetic beads	Merck Millipore	16-663
Albumin Fraction V	Carl Roth	8076.4
BCA Protein Assay Kit	Pierce	23227
CDDO	Biomol	Cay81035
Cell Titer-Glo Luminescent Cell Viability Assay	Promega	G7571
CytoTox 96® Lactate Dehydrogenase Assay	Promega	#G1780

Enhanced chemiluminescence (ECL) Western Blotting Detection Reagent	GE Healthcare	RPN2106
Ethanol absolute	Merck	100983
Fetal bovine serum (FBS)	Thermo Fisher Scientific	10270-106
Formaldehyde, 16%	Thermo Fisher Scientific	28908
Gentamicin	Life Technologies	15750037
Glycerol	Carl Roth	4626.4
IL-1β ELISA kit	R&D Systems	DY401
Image-iT® R FX signal enhancer	Invitrogen	I36933
LEAF Purified anti-mouse IFN-β Antibody	Biolegend	508104
LEAF Purified Syrian Hamster IgG Isotype Control Antibody	Biolegend	400916
Lipofectamine 3000 transfection reagent	Thermo Fisher Scientific	L3000-008
Methanol	Carl Roth	4627.6
MitoSOX Mitochondrial ROS Detection Kit	Thermo Fisher Scientific	M36008
NE-PER Nuclear and Cytoplasmic Extraction Kit	Thermo Fisher Scientific	78833
Normal goat serum	Life Technologies	PCN5000
Opti-MEM Reduced Serum Medium, GlutaMAX Supplement	Thermo Fisher Scientific	51985034
Phosphate-buffered saline (PBS)	Merck Millipore	L1825
ProLong Gold antifade containing DAPI	Life Technologies	P36935
Protease & Phosphatase Inhibitor Cocktail	Thermo Fisher Scientific	1861280
RNeasy Mini Kit	Qiagen	74106
Seahorse XF Cell Mito Stress Test Kit	Agilent	103015-100
Sodium dodecyl sulfate (SDS)	Carl Roth	0.183.3
SsoFast EvaGreen Supermix	Bio-Rad	1725201
SuperScript III reverse transcriptase	Thermo Fisher Scientific	18080-044
Tetramethylrhodamine methyl ester (TMRM)	Thermo Fisher Scientific	T-668

Trigonelline hydrochloride	Merck	T5509
Tris-HCl	Carl Roth	9090.2
Triton X-100	Carl Roth	3051.3
Trypan blue stain 0.4%	Thermo Fisher Scientific	15250061
Tween 20	Carl Roth	9127.1
VLE RPMI 1640 cell culture medium	Merck Millipore	FG1415

2.1.4   List of antibodies

Antibody	Company	Cat. Number
Alexa Fluor 488 anti-mouse IgG	Invitrogen	A-11017
Alexa Fluor 488 anti-rabbit IgG	Invitrogen	A-11008
Alexa Fluor 594 anti-rabbit IgG	Invitrogen	A-11072
Anti-mouse IgG HRP-conjugated	R&D Systems	HAF007
Anti-rabbit IgG HRP-conjugated	R&D Systems	HAF008
β-actin	Santa Cruz	sc-47778
GAPDH	Santa Cruz	sc-47724
Keap1	Proteintech	10503-2-AP
Lamin B	Santa Cruz	sc-374015
LC3	Sigma Aldrich	L7543
MLKL	Santa Cruz	sc-165025
Nrf2	Santa Cruz	sc-722
p70 S6 kinase	Cell Signaling	9202
Pgam5	Abcam	ab126534
phospho-p70 S6 kinase	Cell Signaling	9205
phospho-MLKL	Abcam	ab196436
phospho-RIP3	Abcam	ab195117
RIP3	Santa Cruz	sc-135171
SQSTM1/p62	Cell Signaling	5114
Tom20	Santa Cruz	sc-17764

2.2   Methods

2.2.1   Cell culture and bacterial infection

Mice and generation of bone marrow-derived macrophages

Bone marrow was extracted from 8 to 12 weeks old wildtype C57BL/6 (WT), type I interferon receptor (*Ifnar1*^{-/-}), autophagy-related protein 7 (*Atg7*^{-/-}) and receptor-interacting serine/threonine-protein kinase 3 (*RIP3*^{-/-}) deficient mice. Bone marrow was differentiated into macrophages in RPMI medium supplemented with 10% of fetal bovine serum (FBS) and 20% of L929 cell culture supernatant for 7 days in a humidified incubator at 37°C and 5% CO_2. Non-adherent cells were removed on days 3 and 5 and adherent bone marrow-derived macrophages (BMDMs) were used for experiments from day 7 to 9. All animal studies were performed according to institutional guidelines on animal welfare and were approved by the North Rhine-Westphalian State Agency for Nature, Environment, and Consumer Protection (Landesamt für Natur, Umwelt and Verbraucherschutz [LANUV] Nordrhein-Westfalen; File no: 84-02.05.40.14.082 and 84-02.04.2015.A443) and the animal care committee of the University of Cologne.

S. Typhimurium infection of macrophages

Salmonella enterica serovar Typhimurium (SL1344) was grown to the late-exponential phase in Brain Heart Infusion (BHI) broth at 37°C with constant agitation. Bacteria were then harvested, resuspended in 10% of sterile glycerol and aliquots were stored at -80°C until further use. For all experiments, BMDMs were infected with a multiplicity of infection (MOI) of 10 for 10 min at room temperature and 30 min at 37°C. Subsequently, extracellular bacteria were removed by three times washing with RPMI medium containing 50 µg/ml gentamicin. Afterwards, infected BMDMs were incubated with RPMI medium containing 10% FBS and 50 µg/ml gentamicin at 37°C. After 2 h of infection, gentamicin was diluted to 10 µg/ml for the remainder of the experiment. At the desired time points, BMDMs were washed once with PBS and samples were collected for experiments.

Bacterial colony formation assay

BMDMs (0.5 x 10^6 cells/well) were seeded in 6-well plates 24 h prior to infection with *S.* Typhimurium. At 0 h and 24 h post infection, BMDMs were lysed with 1% Triton X-100 and 0.01% SDS/PBS solution and samples were collected in 1.5 ml Eppendorf tubes. Lysates were serially diluted with sterile PBS and spread on BHI agar plates, which were incubated overnight at 37°C. The next day, colony forming units (CFUs) were counted to determine the number of intracellular bacteria.

2.2.2 Protein and enzymatic assays

Immunoblot analysis

BMDMs (1.0-2.0 x 10^6 cells/well) were lysed with radio-immunoprecipitation assay (RIPA) buffer containing protease and phosphatase inhibitors and the protein amount of each sample was quantified using the BCA Protein Assay Kit according to the manufacturer`s instructions. Equal amounts of protein were mixed with SDS-PAGE sample loading buffer, boiled, resolved by SDS-PAGE and proteins were transferred to a PVDF membrane. Next, membranes were blocked with either 5% milk or 5% bovine serum albumin (BSA) in tris buffered saline (TBS) containing 0.05% Tween 20 (TBS-Tween) for 1 h at room temperature. Membranes were then incubated overnight at 4°C with primary antibodies against LC3, p70 S6 kinase, phospho-p70 S6 kinase, SQSTM1/p62, Tom20, Nrf2, β-actin, Keap1, MLKL, phospho-MLKL, RIP3, phospho-RIP3, or Pgam5 diluted in TBS-Tween containing either 5% milk or 5% BSA. After three times washing with TBS-Tween, membranes were incubated with the appropriate secondary antibody conjugated to horseradish peroxidase (HRP) for 1 h at room temperature. Membranes were washed three times with TBS-Tween and incubated with an enhanced chemiluminescence (ECL) substrate for 1 min at room temperature and exposed to a X-ray film. X-ray films were automatically developed using the Curix60 machine (Agfa). Densitometric quantification of western blotting was performed using ImageJ software (NIH).

Immunoprecipitation

BMDMs were plated in 10 cm dishes at 5.0 x 10^6 cells per dish 24 h before the experiment. BMDMs were infected with *S.* Typhimurium and samples were lysed with RIPA buffer containing protease and phosphatase inhibitors. After preclearing the cell lysate with protein A/G agarose magnetic beads for 1 h, beads were removed by placing the tube on a magnetic rack. The whole cell lysate (approximately 500 µg of protein) was incubated with 4 µg of an antibody against Nrf2 overnight at 4°C. Protein A/G agarose beads were added again and incubated for an additional 1 h at room temperature. The immunoprecipitated proteins along with the agarose beads were collected by placing the tube on a magnetic rack. The collected beads were washed five times with RIPA buffer. Samples were mixed with SDS-PAGE sample loading buffer, boiled and resolved on a 10% SDS-polyacrylamide gel. The respective proteins precipitated were identified by immunoblot analysis.

Subcellular fractionation analysis

Nuclear fractions from BMDMs (1.0 x 10^6 cells/well) seeded in 6-well plates 24 h prior to infection were prepared using the NE-PER Nuclear and Cytoplasmic Extraction Kit according to the manufacturer's instructions. Samples were subjected to SDS-PAGE and analyzed by immunoblotting with antibodies against Nrf2, Lamin B, or GAPDH.

Enzyme-linked immunosorbent assay (ELISA)

BMDMs (0.5-1.0 x 10^6 cells/well) were seeded in 6-well plates 24 h prior to infection. For ELISA, cell culture supernatants were collected 6 h and 24 h post infection and were kept at -80°C until assayed for mouse IL-1β according to manufacturer´s instructions. Absorbance was measured with a multimode plate reader at 450 nm (PerkinElmer).

2.2.3 Mitochondrial and cell viability assays

Mitochondrial ROS detection

Mitochondrial reactive oxygen species (mtROS) were determined using MitoSOX according to the manufacturer´s instruction. BMDMs (0.5 x 10^6 cells/well) were seeded in 12-

well plates 24 h prior to the experiment and were infected with *S.* Typhimurium for 6 h. Samples were subsequently fixed with 1% (wt/vol) formaldehyde in PBS for 10 min at room temperature and were then collected in FACS tubes. Fluorescence intensity of 50,000 cells per sample was analyzed by gating on live cells using the BD FACSCanto flow cytometer and FLOWJO software (Tree Star). The fluorescence intensity of BMDMs treated with MitoSOX was normalized to the intensity of BMDMs without MitoSOX treatment.

Measurement of mitochondrial membrane potential

Mitochondrial membrane potential (Ψm) was analyzed by TMRM staining, which is a fluorescent dye that accumulates in active mitochondria with intact mitochondrial membrane potentials. BMDMs (0.5×10^6 cells/well) were seeded in 12-well plates 24 h prior to the experiment and BMDMs were subsequently infected with *S.* Typhimurium. After 6 h of infection, medium was exchanged to fresh RPMI medium containing 10% FBS and 10 µM of TMRM. BMDMs were incubated with TMRM for 10 min at room temperature. Next, cells were washed three times with PBS, samples were fixed with 1% (wt/vol) formaldehyde in PBS for 10 min at room temperature and were then collected in FACS tubes. Fluorescence intensity of 50,000 cells per sample was analyzed by gating on live cells using the BD FACSCanto flow cytometer and FLOWJO software (Tree Star). The fluorescence intensity of BMDMs treated with TMRM was normalized to the intensity of BMDMs without TMRM treatment.

Seahorse assay

Oxygen consumption rate (OCR) was analyzed using the Seahorse XF Cell Mito Stress Test Kit according to manufacturer's instruction. Briefly, BMDMs were seeded at 0.2×10^5 cells/well in a 96-well Seahorse plate 24 h before the experiment. A utility plate containing equilibration solution was placed in a CO_2-free incubator at 37°C overnight. The following day, media was removed and cells were infected with *S.* Typhimurium as described before. After 2 h of infection, medium was replaced with glucose, glutamine and sodium pyruvate-supplemented XF assay buffer and the plate was placed in a CO_2-free incubator for at least 30 min. Inhibitors (Oligomycin, carbonyl cyanide-4-(trifluoromethoxy)phenylhydrazone

[FCCP], 2-Deoxy-D-glucose [2DG], Rotenone) were added to the appropriate port of the injector plate. After calibration with the utility plate, the sample plate was run on the Seahorse XF-96 machine.

ATP measurement

BMDMs were seeded at 0.1 x 10^6 cells/well in a 96-well plate 24 h before infection with *S*. Typhimurium. After 2 h and 6 h of infection, ATP levels were determined using the Cell Titer-Glo Luminescent Cell Viability Assay according to manufacturer's instructions. Luminescence was measured with a multimode plate reader (PerkinElmer).

Cell viability assay

BMDMs were seeded into a 96-well plate at 0.1 x 10^6 cells/well 24 h prior to the experiment. BMDMs were infected with *S*. Typhimurium and cell viability was measured at 2 h and 6 h post infection using the CytoTox 96® Lactate Dehydrogenase Assay (LDH) according to the manufacturer's instructions. Luminescence was determined with a multimode plate reader (PerkinElmer).

2.2.4 Microscopic analyses

Immunofluorescent staining and confocal microscopy

BMDMs (0.1 x 10^6 cells/well) were seeded in 24-well plates containing 12 mm round coverslips 24 h before infection. After infection with *S*. Typhimurium, BMDMs were fixed with 4% (wt/vol) formaldehyde in PBS for 15 min at room temperature. BMDMs were washed with PBS and permeabilized with 0.3% Triton X-100 in PBS for 5 min at room temperature. Next, BMDMs were washed with 0.03% Triton X-100 in PBS followed by incubation with Image-iT® R FX signal enhancer for 30 min and blocking with 5% BSA, 5% normal goat serum and 0.03% Triton X-100 in PBS (blocking buffer) for 1 h at room temperature. After washing with 0.03% Triton X-100 in PBS, BMDMs were incubated overnight at 4°C with primary antibodies against SQSTM1/p62, Tom20, Nrf2, Keap1, or Pgam5 diluted in blocking buffer. BMDMs were then washed three times with 0.03% Triton X-100 in PBS and incubated with appropriate

24

fluorescent secondary antibodies diluted in blocking buffer for 1 h at room temperature. After three times washing with 0.03% Triton X-100 in PBS, coverslips were mounted on glass slides using ProLong® Gold antifade containing DAPI and stored at 4°C until image acquisition. Images were acquired with a 60X oil PlanApo objective, numerical aperture 1.4 at room temperature on an Olympus IX81 inverted confocal microscope equipped with PMT detectors for imaging. Olympus Fluoview FV10-ASW 4.2 software was used for acquisition and calculating Pearson's correlation.

Electron microscopy

BMDMs (1.5×10^6 cells/well) were fixed (2.5% glutardehyde, 2.5% sucrose, 3 mM calcium chloride, 100 mM HEPES, pH 7.4) for 1 h at room temperature. After washing with 0.1 M cacodylate buffer (pH 7.2), cells were scraped and collected in cacodylate buffer. Cells were centrifuged (5 min, 500 x g, room temperature) and resuspended in 500 µl of warm 3% low melting agarose (diluted in cacodylate buffer). Cell suspension was transferred into a sealed 1 ml tip, placed into a 15 ml falcon tube and centrifuged at 1.500 x g for 10 min at room temperature to concentrate cells. The agarose pellet was removed from the tip and collected into 0.1 M cacodylate buffer. After fixation, cells were dehydrated in graded ethanol series (50%, 70%, 90%, 100%) for 3 min each and were then incubated with ethanol and propylenoxid. Next, cells were embedded using Epon medium. Sections were cut at a thickness of 70 nm (Ultracut UC6, Leica), stained with 1.5% aqueous uranyl acetate for 15 min at 37°C and contrasted using lead nitrate solution. Samples were examined with an EM109 electron microscope (Zeiss) and images were recorded at 7,000 x or 50,000 x magnification.

2.2.5 mRNA assays

Transfection experiments

BMDMs (1.0×10^6 cells/well) were seeded in a 6-well plate 24 h prior to transfection and were incubated with either 50 nM of non-targeting siRNA (#SR-CL000-005, Eurogentec)

or 50 nM of siRNA specific for *Nfe2l2* (Nrf2; #L-040766-00-0005, Dharmacon), *Sqstm1* (p62; #L-047628-01-0005, Dharmacon), or *Pgam5* (#L-052506-01-0005, Dharmacon) together with the transfection reagent Lipofectamine 3000 according to manufacturer's instructions. Briefly, for each well 0.5 µl of siRNA (100 µM) was diluted in 50 µl of Opti-MEM medium and was added to 4 µl of Lipofectamine transfection reagent diluted in 50 µl of Opti-MEM medium. Samples were gently mixed and incubated for 10 min at room temperature. Next, 100 µl of the transfection mix was added drop by drop to each well, which contained 900 µl of RPMI medium supplemented with 10% of FBS. After 5 to 6 h of incubation at 37°C, the medium was exchanged to RPMI containing 10% of FBS. At 48 h post transfection, BMDMs were infected with *S*. Typhimurium. Knockdown efficiency was individually assessed by immunoblot analyses using antibodies against Nrf2, p62, or Pgam5.

Quantitative real-time PCR (qRT-PCR)

Total RNA from BMDMs (1.0×10^6 cells/well) was isolated by RNeasy Mini Kit and cDNA (500 ng) was synthesized with random hexamers using reverse transcriptase (SuperScript III). Primers were designed using Primer3 software and Basic Local Alignment Search Tool (National Center for Biotechnology Information, Bethesda, MD). PCR reactions (25 µL) contained 10 ng of cDNA, 0.4 µmol/L of each forward and reverse primer, and master mix (SsoFast EvaGreen Supermix). Real-time PCR was performed on a PCR Cycler CFX96 (Bio-Rad) under the following conditions: initial denaturation step of 95°C for 2 min, 40 cycles of 95°C for 5 sec and 60°C for 15 sec, followed by a denaturation step of 95°C for 60 sec and subsequent melt curve analysis to check amplification specificity. Results were analyzed by the comparative threshold cycle method with hypoxanthine-guanine phosphoribosyltransferase (*Hprt*) as the endogenous reference gene for all reactions. The relative mRNA levels of uninfected BMDMs were used as normalized controls for infected BMDMs. All assays were performed in triplicates, and a non-template control was included in all experiments to exclude DNA contamination. Primers were obtained from Invitrogen and are listed in **Tab. 1**.

Gene	Primer sequence
Lc3b (for)	5'-TCATGGACTGAAGCCAGCATAG-3'
Lc3b (rev)	5'-TAGCAAAGACAGCTGCATGC-3'
Sqstm1/p62 (for)	5'-AAACATGGTGCACCCCAATG-3'
Sqstm1/p62 (rev)	5'-AGATGAGCTTGCTGTGTTCC-3'
Lamp1 (for)	5'-AGTCTTGTGTTGGCGTTCAG-3'
Lamp1 (rev)	5'-AGGCAATGCATTACGTGAGC-3'
Nqo1 (for)	5'-AGCGTTCGGTATTACGATCC-3'
Nqo1 (rev)	5'-AGTACAATCAGGGCTCTTCTCG-3'
Hmox-1 (for)	5'-GGTCAGGTGTCCAGAGAAGG-3'
Hmox-1 (rev)	5'-CTTCCAGGGCCGTGTAGATA-3'
Gclc (for)	5'-GTGGACGAGTGCAGCAAG-3'
Gclc (rev)	5'-GTCCAGGAAATACCCCTTCC-3'
Hprt (for)	5'-GTTGGATACAGGCCAGACTTTGTTG-3'
Hprt (rev)	5'-GATTCAACTTGCGCTCATCTTAGGC-3'
IL-1β (for)	5'-GTCCTGTGTAATGAAAGACGGC-3'
IL-1β (rev)	5'-CTGCTTGTGAGGTGCTGATGTA-3'

Table 1. List of primers used in this study. for, forward. rev, reverse.

2.2.6 Statistical analyses

Statistical analyses were performed using Prism software (GraphPad, version 5). Differences between groups were assessed by two-tailed unpaired Student´s t test or One-way ANOVA with repeated measures when more than two groups were analyzed. Every single experiment was repeated at least three times. Unless otherwise specified, results are presented as mean ± standard deviation (SD). Differences were considered statistically significant when $p \leq 0.05$ (*), very significant when $p \leq 0.01$ (**), and highly significant when $p \leq 0.001$ (***).

3.   Results

3.1   *S.* Typhimurium induces IFN-I signaling pathways in macrophages

To investigate whether IFN-I signaling plays a role upon *S.* Typhimurium infection of macrophages, bone-marrow derived macrophages (BMDMs) from wild-type (WT) and IFN-I receptor deficient (*Ifnar1$^{-/-}$*) mice were infected with *S.* Typhimurium and supernatants were subsequently analyzed by ELISA for IFN-β secretion. As shown in **Fig. 1 A**, *S.* Typhimurium infection induced the secretion of IFN-β, which is the major IFN-I secreted by murine macrophages, 6 hours (h) post infection (p.i.) in both WT and *Ifnar1$^{-/-}$* BMDMs to a similar level. In *S.* Typhimurium-infected WT BMDMs, secreted IFN-β lead to the phosphorylation of the transcription factors STAT1 and STAT3, which are located downstream of the IFN-I receptor (Ifnar1). By contrast, phosphorylation of STAT1 and STAT3 was markedly reduced in infected *Ifnar1$^{-/-}$* BMDMs as determined by immunoblot analysis (**Fig. 1 B**). These results demonstrate that *S.* Typhimurium infection induces the secretion of IFN-β that leads to auto- and paracrine engagement of Ifnar1 resulting in the activation of downstream IFN-I signaling pathways.
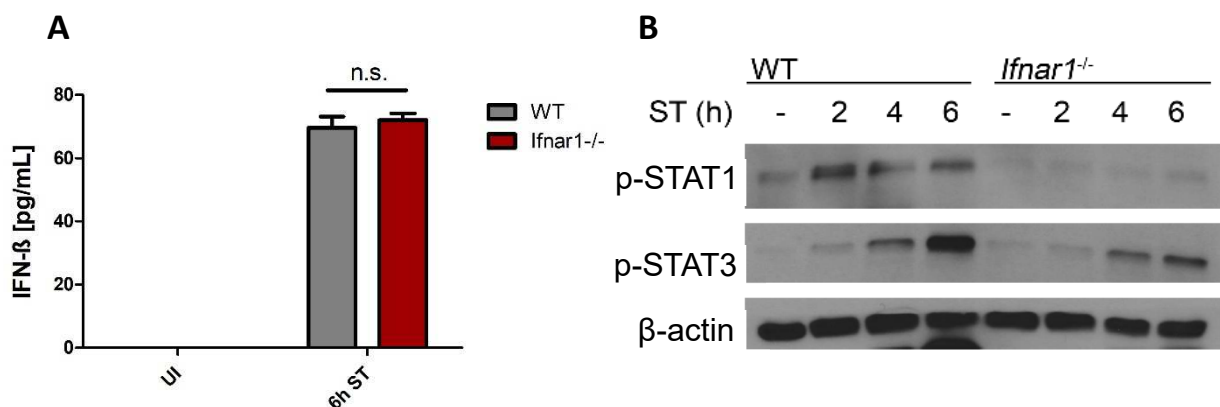

Figure 1. *S.* Typhimurium infection induces IFN-I signaling pathways in macrophages.

(A) Analysis of IFN-I secretion by ELISA. Supernatants of WT and *Ifnar1$^{-/-}$* BMDMs were analyzed for IFN-β secretion, which is the predominant IFN-I in mice, 6 h after infection with *S.* Typhimurium (ST). UI, uninfected.

(B) Immunoblot analysis of Ifnar1-dependent pathways. Phosphorylation of the transcription factors STAT1 and STAT3 was analyzed in total cell lysates of WT and *Ifnar1$^{-/-}$* BMDMs at the indicated time points after infection with *S.* Typhimurium (ST). STAT1 and STAT3 function downstream of Ifnar1. p, phosphorylated.

3.2 *S.* Typhimurium induces IFN-I-mediated cell death of macrophages

Previous work from our group has demonstrated that *S.* Typhimurium causes necroptotic cell death of macrophages, which was dependent on IFN-I signaling (Robinson et al. 2012). To confirm this finding, WT and *Ifnar1*^{-/-} BMDMs were infected with S. Typhimurium and cell death was assessed 6 h p.i. In line with our previous findings, *S.* Typhimurium infection caused significantly more cell death in WT BMDMs compared to *Ifnar1*^{-/-} BMDMs (**Fig. 2 A**). Furthermore, we determined the amount of cellular ATP, which has commonly been used as a marker for cell viability, and found that *S.* Typhimurium infection reduced ATP levels of both WT and *Ifnar1*^{-/-} BMDMs 2 h and 6 h p.i. (**Fig. 2 B**). When compared to infected *Ifnar1*^{-/-} BMDMs, however, ATP levels were significantly lower in *S.* Typhimurium-infected WT BMDMs. These results therefore indicate that *S.* Typhimurium infection causes cell death and reduces energy levels of macrophages, which is further enhanced by IFN-I signaling.
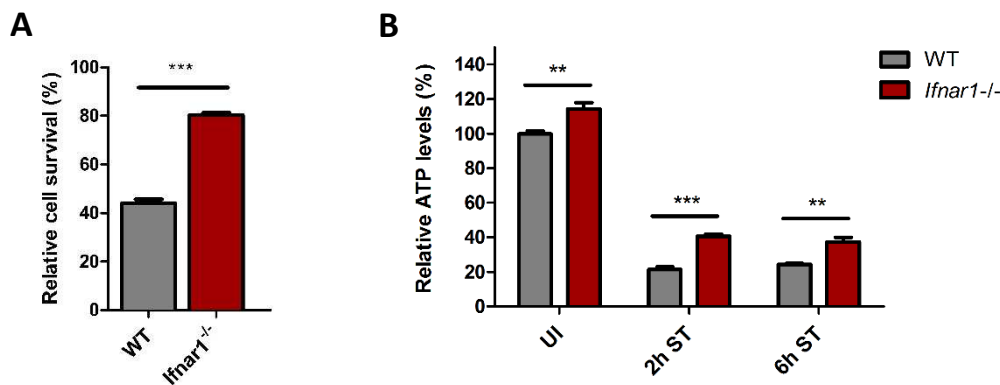
Figure 2. IFN-I signaling exacerbates *S.* Typhimurium-induced cell death of macrophages.

(A) Luminescence analysis of IFN-I-dependent cell death. Luminescence signals of WT and *Ifnar1*^{-/-} BMDMs were assessed to determine cell viability 6 h after *S.* Typhimurium infection. Values were normalized to the luminescence signal of uninfected WT BMDMs.

(B) Luminescence analysis of relative ATP levels. WT and *Ifnar1*^{-/-} BMDMs were infected with *S.* Typhimurium (ST) for the indicated time and the luminescence signals were measured to determine the amount of ATP. Values were normalized to ATP levels of uninfected (UI) WT BMDMs. Figure taken from (Hos et al. 2017).

3.3 IFN-I signaling exacerbates *S.* Typhimurium-induced mitochondrial damage

Next, we sought to analyze the upstream events leading to *S.* Typhimurium-induced cell death of macrophages. As mitochondrial dysfunction has been identified as a major cause for cell death (Galluzzi et al. 2012), we first investigated whether mitochondrial damage precedes *S.* Typhimurium-induced cell death and whether mitochondrial dysfunction is dependent on IFN-I signaling.

Using immunofluorescence microscopy, we assessed mitochondrial morphology in uninfected and *S.* Typhimurium-infected WT and *Ifnar1*^{-/-} BMDMs stained with an antibody against the mitochondrial outer membrane protein Tom20. Uninfected WT and *Ifnar1*^{-/-} BMDMs showed the typical tubular mitochondrial network, whereas WT and *Ifnar1*^{-/-} BMDMs infected with *S.* Typhimurium for 6 h displayed increased mitochondrial fragmentation, indicative of mitochondrial damage (**Fig. 3 A**). Compared to *Ifnar1*^{-/-} BMDMs, however, the integrity of the mitochondrial network appeared more disrupted in infected WT BMDMs. Consistently, electron microscopy revealed accumulation of damaged mitochondria in *S.* Typhimurium-infected WT BMDMs, whereas mitochondrial integrity was better conserved in *Ifnar1*^{-/-} BMDMs 6 h p.i. (**Fig. 3 B**).
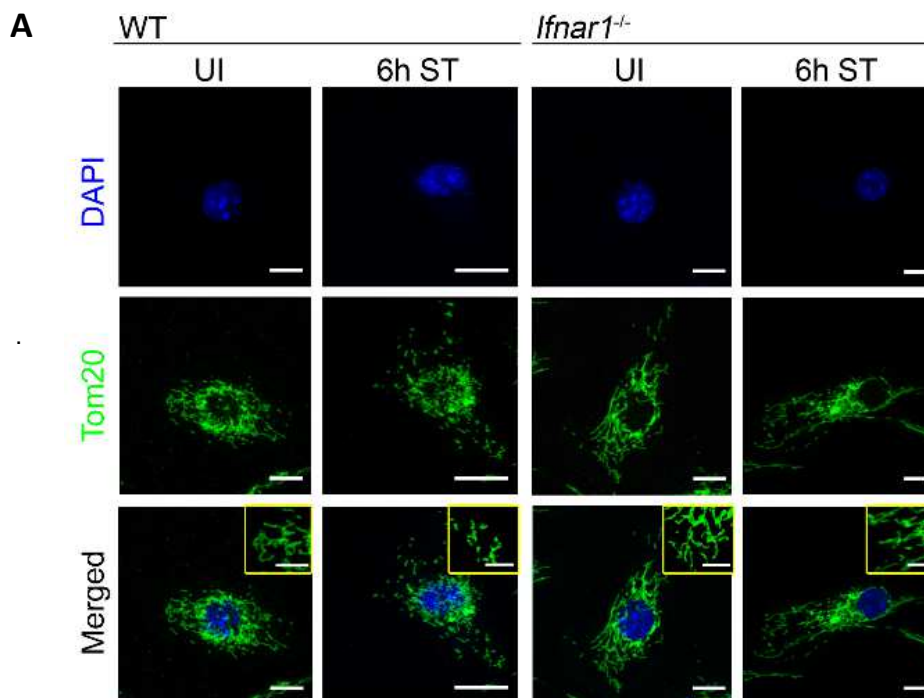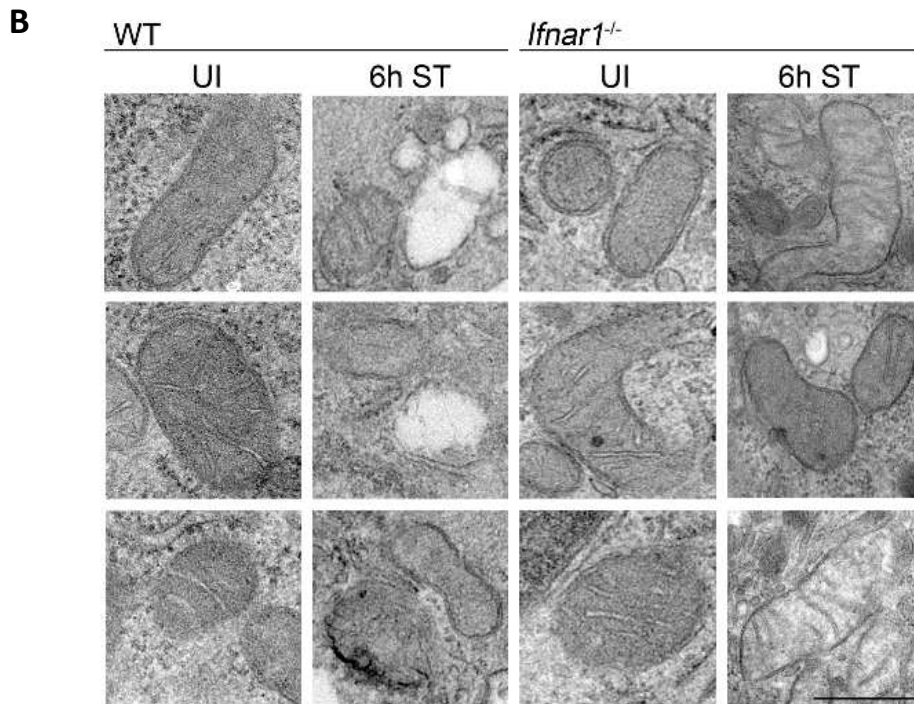
Figure 3. IFN-I signaling exacerbates *S.* Typhimurium-induced mitochondrial damage.

(A) Immunofluorescence staining of mitochondrial network. WT and *Ifnar1*^{-/-} BMDMs were infected with *S.* Typhimurium (ST) for 6 hours, immunostained for Tom20 (green) and examined by confocal microscopy (scale bars, 10 µm). Each inset represents a magnified image (scale bars, 4 µm). UI, uninfected.

(B) Electron micrographs of mitochondria. Shown are three representative examples of mitochondria in uninfected (UI) or *S.* Typhimurium (ST)-infected WT and *Ifnar1*^{-/-} BMDMs. Scale bar represents 250 nm.

Figures taken from (Hos et al. 2017).

Enhanced mitochondrial damage in WT BMDMs correlated with increased mitochondrial ROS (mtROS) production as determined by MitoSOX staining and decreased mitochondrial membrane potential (ψm) analyzed by TMRM fluorescence intensity. By contrast, *S.* Typhimurium-infected *Ifnar1*^{-/-} BMDMs generated less mtROS consistent with sustained ψm (**Fig. 4, A-C**). Mitochondrial function was further assessed by analyzing the oxygen consumption rate (OCR) of *S.* Typhimurium-infected WT and *Ifnar1*^{-/-} BMDMs using seahorse assay. As shown in **Fig. 4 D**, *S.* Typhimurium infection reduced the OCR in both WT and *Ifnar1*^{-/-} BMDMs. However, the OCR was significantly lower in WT BMDMs compared to *Ifnar1*^{-/-} BMDMs 6 h p.i.
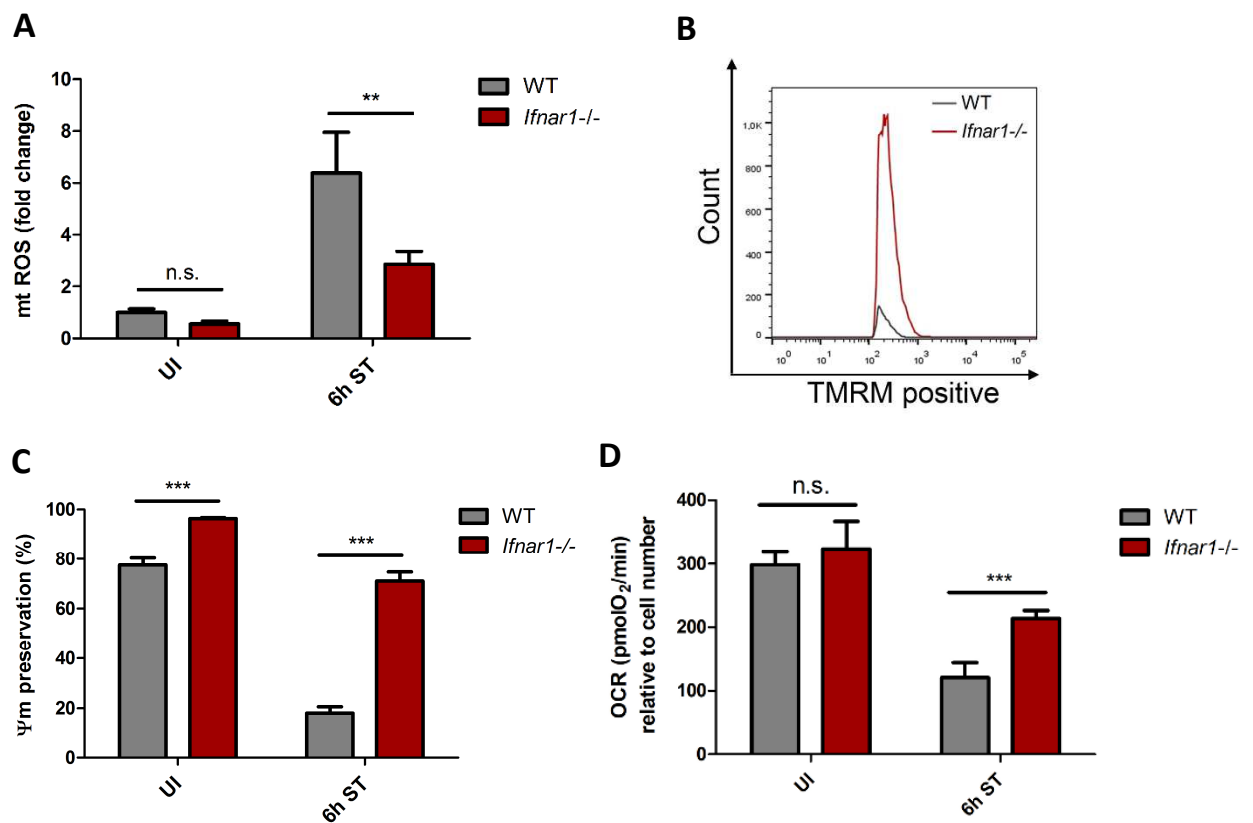
Figure 4. IFN-I signaling impairs mitochondrial function in *S.* Typhimurium-infected macrophages.

(A) Relative mitochondrial reactive oxygen species (mtROS) production. WT and *Ifnar1*$^{-/-}$ BMDMs were infected with *S.* Typhimurium (ST) for 6 h and the amounts of mtROS relative to uninfected (UI) WT BMDMs were analyzed by FACS using MitoSOX staining.

(B) Flow cytometric analysis of mitochondrial membrane potential (ψm). WT and *Ifnar1*$^{-/-}$ BMDMs were infected with *S.* Typhimurium (ST) for 6 h and the number of TMRM positive cells was measured by flow cytometry. TMRM leaks from damaged mitochondria resulting in a loss of fluorescent intensity.

(C) Quantification of mitochondrial membrane potential (ψm). ψm of uninfected (UI) and *S.* Typhimurium (ST)-infected WT and *Ifnar1*$^{-/-}$ BMDMs was determined as described in (B) and changes of ψm from three independent experiments were subsequently quantified.

(D) Measurement of relative oxygen consumption rate (OCR). Relative OCR was analyzed in WT and *Ifnar1*$^{-/-}$ BMDMs 6 h after *S.* Typhimurium (ST) infection by seahorse assay. The OCR was normalized to total cell numbers of WT and *Ifnar1*$^{-/-}$ BMDMs, respectively. UI, uninfected.

Figures taken from (Hos et al. 2017).

Furthermore, Tom20 expression, which has commonly been used as a marker for mitochondrial mass, was distinctly decreased in WT BMDMs 6 h after infection, whereas Tom20 levels remained unchanged in *Ifnar1*$^{-/-}$ BMDMs (**Fig. 5, A and B**). Taken together, these findings demonstrate that *S.* Typhimurium infection causes mitochondrial damage in macrophages. Importantly, IFN-I signaling further enhances mitochondrial dysfunction upon *S.* Typhimurium infection of macrophages.

A   **B**
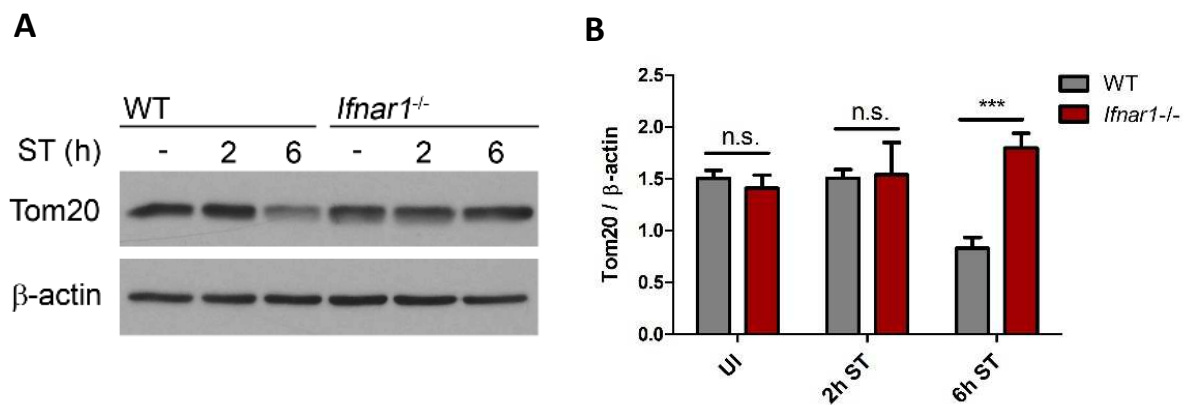
Figure 5. IFN-I signaling decreases mitochondrial mass of *S*. Typhimurium-infected macrophages.

(A) Immunoblot analysis of mitochondrial mass. WT and *Ifnar1*^{-/-} BMDMs were infected with *S*. Typhimurium (ST) for the indicated time and total cell lysates were immunostained for Tom20 as a marker for mitochondrial mass.

(B) Relative Tom20 expression was determined by densitometric quantification from three independent immunoblots. UI, uninfected; ST, *S*. Typhimurium.

Figures taken from (Hos et al. 2017).

3.4   IFN-I-mediated mitochondrial damage and energy depletion transiently triggers autophagy

As mitochondria are the main sources of cellular ATP, damage of mitochondria interferes with cellular energy homeostasis and eventually results in energy depletion. Many studies have convincingly shown that reduced energy levels lead to the activation of autophagy, which enables the cell to restore energy homeostasis by recycling cellular organelles and protein aggregates through lysosomal degradation (Deretic et al. 2013; Mizushima et al. 2008).

Having shown that *S*. Typhimurium infection causes mitochondrial damage and energy depletion in macrophages, we next investigated whether reduced ATP levels trigger autophagy. Indeed, electron microscopy revealed that 2 h after *S*. Typhimurium infection autophagosomes were formed in both WT and *Ifnar1*^{-/-} BMDMs (**Fig. 6 A**). To assess autophagic activity more precisely, we determined the expression levels of the autophagic adaptor protein p62 and the autophagic marker proteins LC3-I and LC3-II following *S*. Typhimurium infection of macrophages. P62 and autophagosome-associated LC3-II

(lipidated form) are degraded along with the autolysosome and their amounts are therefore inversely correlated with autophagic flux. As shown in **Fig. 6 B**, *S.* Typhimurium infection induced the expression of p62 and LC3 in WT and *Ifnar1*^{-/-} BMDMs at 2 h, 4 h and 6 h p.i. as determined by immunoblot. Of note, *S.* Typhimurium infection transiently induced LC3-I to LC3-II conversion in WT BMDMs (2 h p.i.), indicative of autophagy induction, while LC3-I to LC3-II conversion rates were markedly attenuated after 4 h and 6 h of infection, respectively, indicative of blocked autophagic flux. By contrast, autophagic flux was constantly reduced in *S.* Typhimurium-infected *Ifnar1*^{-/-} BMDMs, as shown by a low LC3 I to II conversion rate and a strong accumulation of p62 (4 h and 6 h p.i.; **Fig. 6, C and D**).
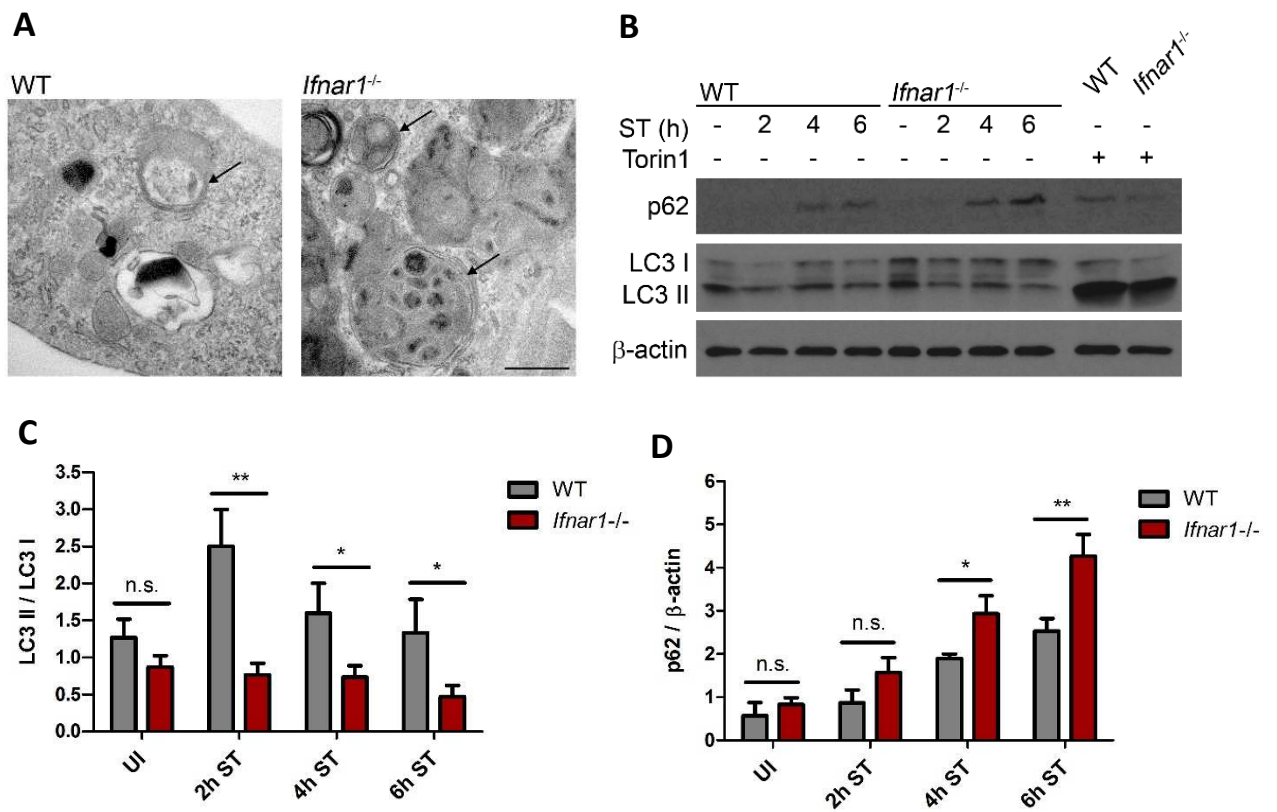
**Figure 6. Mitochondrial damage results in the transient induction of autophagy.**

(A) Electron micrographs of autophagosome formation in *S.* Typhimurium-infected WT and *Ifnar1*^{-/-} BMDMs (2 h p.i.). Arrows point to double-membrane structures indicative of autophagosome formation. Scale bar, 500 nm.

(B) Immunoblot analysis of autophagy marker proteins. WT and *Ifnar1*^{-/-} BMDMs were infected with *S.* Typhimurium (ST) for the indicated time or treated with Torin1 (10 µM, 4 h), and p62 and LC3 expression were determined in total cell lysates by immunoblot. Torin1 inhibits mTORC1 and was used as a positive control for autophagy induction.

(C and D) LC3 I to LC3 II conversion rates **(C)** and relative p62 expression levels **(D)** were determined from three independent immunoblots by densitometric quantification. UI, uninfected. ST, *S.* Typhimurium.

Figures taken from (Hos et al. 2017).

We further confirmed that IFN-I positively regulates autophagy by using a neutralization antibody against murine IFN-β. As shown in **Fig. 7 A**, neutralizing IFN-β during *S.* Typhimurium infection markedly enhanced the accumulation of p62 indicative of reduced autophagy. In fact, p62 levels of WT BMDMs treated with an antibody against IFN-β were similar to the amount of p62 of autophagy-deficient *Atg7$^{-/-}$* BMDMs. Consistent with our observation that *Ifnar1$^{-/-}$* BMDMs showed reduced autophagic activity, mRNA expression levels of *Lc3b* (LC3) and *Lamp1*, a central regulator of lysosomal biogenesis, were also significantly decreased (**Fig. 7, B and C**).
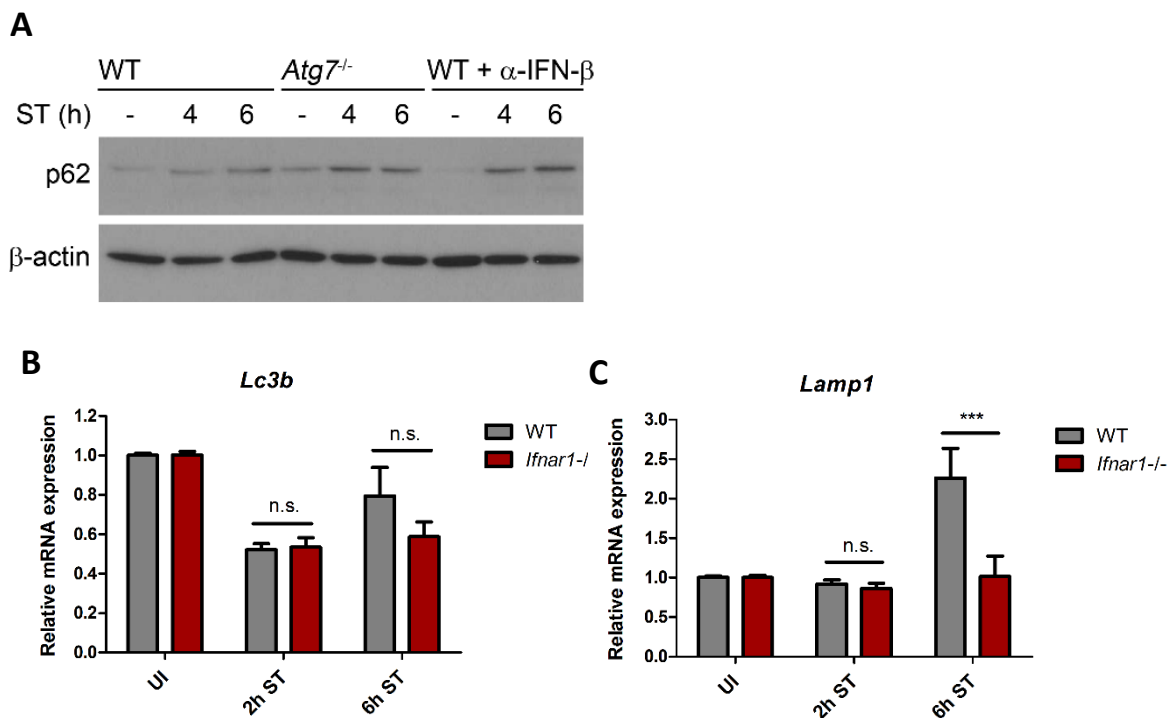

Figure 7. IFN-I signaling transiently induces autophagy in *S.* Typhimurium-infected macrophages.

(A) Immunoblot analysis of p62 expression upon blockade of IFN-I signaling. **P**62 expression was determined in *S.* Typhimurium (ST)-infected WT BMDMs upon neutralization of IFN-β at the indicated time points in comparison to infected WT and *Atg7$^{-/-}$* BMDMs treated with an IgG control. α-IFN-β, anti-IFN-β neutralizing antibody.

(B and C) Relative *Lc3b* and *Lamp1* mRNA expression. WT and *Ifnar1$^{-/-}$* BMDMs were infected with *S.* Typhimurium (ST) for the indicated time and relative **(B)** *Lc3b* and **(C)** *Lamp1* mRNA expression was determined by real-time PCR. Values were normalized to the amounts of mRNA of uninfected (UI) BMDMs.

Figures taken from (Hos et al. 2017).

Importantly, *Ifnar1-/-* BMDMs were not generally deficient in autophagy, since LC3 I to II conversion was observed upon Torin1 treatment, which pharmacologically inhibits mTORC1 activation thereby inducing autophagy (**Fig. 6 B**). Differential autophagy levels in WT and *Ifnar1-/-* BMDMs, however, were not due to altered mTORC1 signaling, as phosphorylation levels of p70 S6 kinase, a downstream target of mTORC1, did not differ significantly (**Fig. 8 A**). Furthermore, transient activation of autophagy did not have a significant effect on the ability of WT BMDMs to clear *S.* Typhimurium compared to infected *Ifnar1-/-* BMDMs (**Fig. 8 B**).
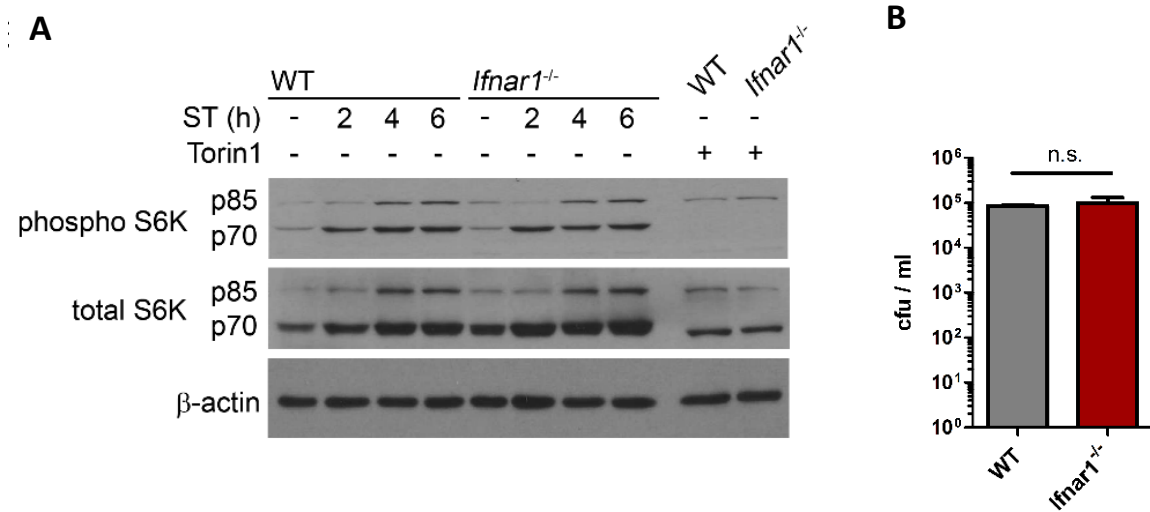
Figure 8. *S.* Typhimurium manipulates autophagy independent of mTORC1.

(A) Immunoblot analysis of mTORC1 activation. Total cell lysates of WT and *Ifnar1-/-* BMDMs infected with *S.* Typhimurium for the indicated time were analyzed for expression and phosphorylation of p70 S6 kinase (S6K) by immunoblot. Phosphorylation of p70 S6K is mediated by mTORC1 and can be inhibited by Torin1 (10 µM, 4 h), which is a pharmacological mTORC1 inhibitor.

(B) Determination of bacterial burden. The number of live bacteria was determined by counting colony forming units (cfu) on agar plates incubated with lysates of WT and *Ifnar1-/-* BMDMs 24 h after infection with *S.* Typhimurium.

Figures taken from (Hos et al. 2017).

Collectively, *S.* Typhimurium infection transiently induces autophagy in macrophages (2 h p.i.), while autophagy is inhibited during the later course of infection (4 h and 6 h p.i.). Importantly, the early induction of autophagy is mediated by IFN-I signaling, while the blockade of autophagy occurs independent of IFN-I signaling. As a result, blockade of autophagy leads to the accumulation of p62 in *S.* Typhimurium-infected macrophages.

3.5   Reduced p62 levels contribute to IFN-I-mediated cell death

As our previous experiments have shown that p62 levels are markedly elevated in *S.* Typhimurium-infected macrophages, we further investigated the functional consequence of p62 accumulation. Recent studies on autophagy-deficient cells have demonstrated that p62 mediates the formation of cytosolic inclusion bodies in response to oxidative stress (Komatsu et al. 2007). Furthermore, p62-positive protein aggregates have been observed during neurodegenerative and chronic liver diseases and have been considered as a pathognomic feature of these diseases (Umemura et al. 2016; Zatloukal et al. 2002).

To investigate whether p62-positive protein aggregates also occur in *S.* Typhimurium-infected macrophages, confocal microscopy on WT and *Ifnar1*^{-/-} BMDMs infected with *S.* Typhimurium for 6 h and stained with an antibody against p62 was performed. Consistent with our immunoblot analyses, p62 expression was also enhanced in *S.* Typhimurium-infected WT BMDMs and p62 levels were even further enhanced in infected *Ifnar1*^{-/-} BMDMs (**Fig. 9, A and B**). Importantly, elevated p62 levels of *Ifnar1*^{-/-} BMDMs were not due to increased *Sqstm1* (the gene encoding p62) mRNA transcription, although a moderate upregulation of *Sqstm1* mRNA was observed in *S.* Typhimurium-infected *Ifnar1*^{-/-} BMDMs compared to WT controls (**Fig. 9 C**).

B

C
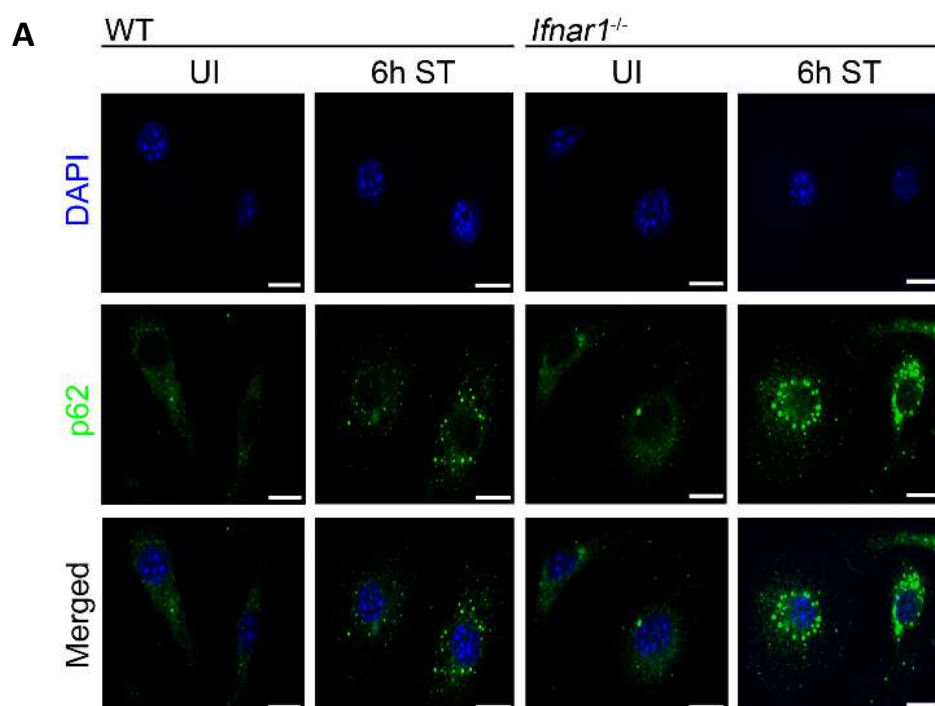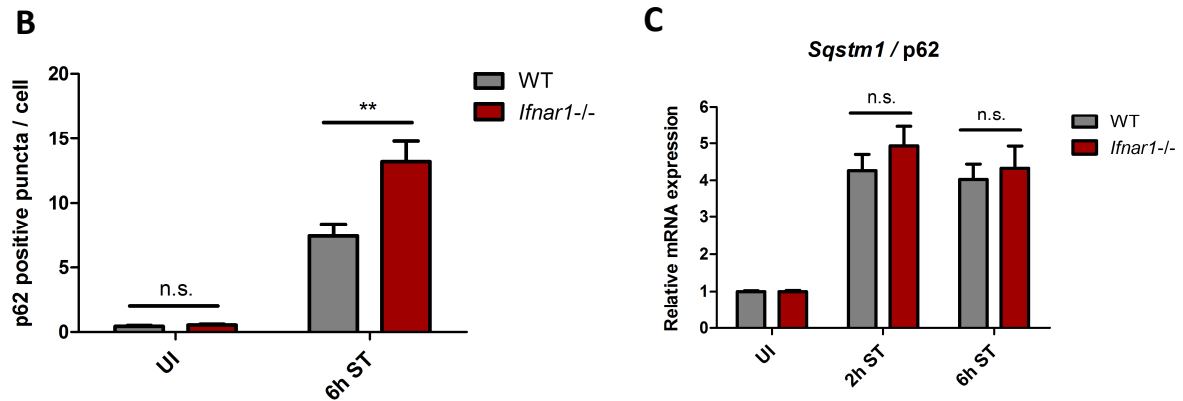
Figure 9. IFN-I signaling decreases p62 levels of *S.* Typhimurium-infected macrophages.

(A) Immunofluorescence staining of p62. After infection with *S.* Typhimurium (ST) for 6 h, WT and *Ifnar1*$^{-/-}$ BMDMs were immunostained for p62 (green) and examined by confocal microscopy (scale bars, 10 µm). UI, uninfected.

(B) Quantification of p62 puncta. The number of p62 positive puncta per cell was quantified in WT and *Ifnar1*$^{-/-}$ BMDMs 6 h after infection with *S.* Typhimurium (ST) (n=50 cells each, repeated for three times). UI, uninfected.

(C) Relative *Sqstm1* (p62*)* mRNA expression. WT and *Ifnar1*$^{-/-}$ BMDMs were infected with *S.* Typhimurium (ST) for the indicated time and *Sqstm1* (the gene encoding p62) mRNA expression was determined by real-time PCR. Values were normalized to the amounts of mRNA in uninfected (UI) BMDMs.

Figures taken from (Hos et al. 2017).

As depicted in **Fig. 9 A**, p62 assembled on large protein aggregates (≥1µm) in the perinuclear region of both WT and *Ifnar1*$^{-/-}$ BMDMs 6 h after *S.* Typhimurium infection. Because of this localization pattern, we reasoned that enhanced p62 levels upon *S.* Typhimurium infection were caused by impaired autophagic degradation of p62. Consistently, pharmacological treatment of infected WT and *Ifnar1*$^{-/-}$ BMDMs with the lysosomal inhibitor Concanamycin A for 4 h and 6 h further elevated p62 levels compared to untreated controls (**Fig. 10, A and B**). Therefore, elevated p62 levels in *S.* Typhimurium-infected macrophages were due to decreased autophagic degradation.
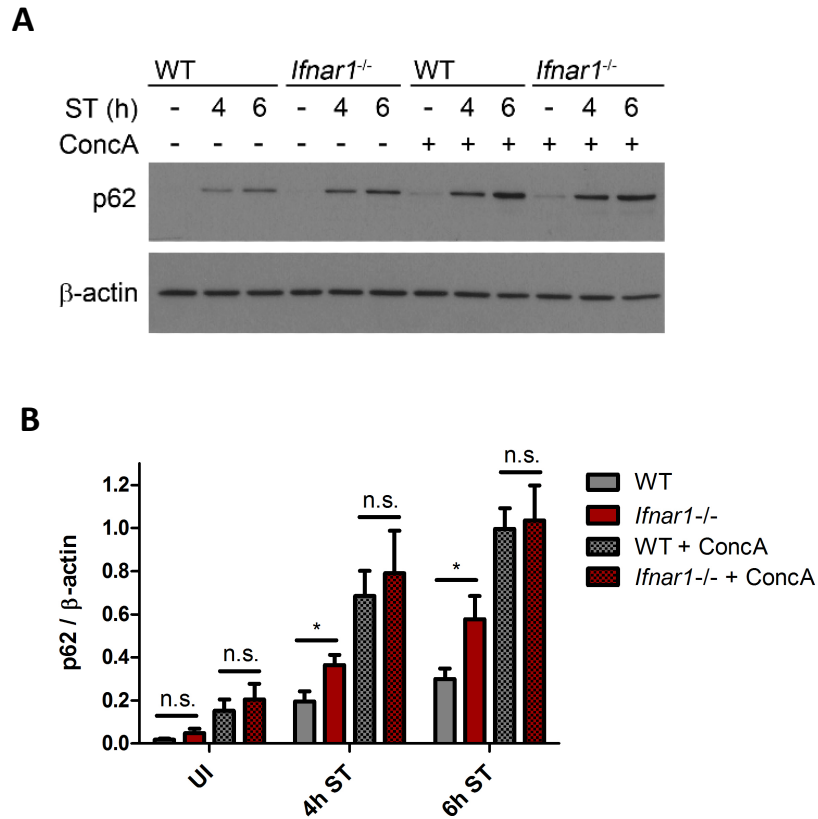
**Figure 10. P62 is degraded through the autophagic pathway.**

(A) Immunoblot analysis of p62 expression upon blockade of autophagy. WT and *Ifnar1-/-* BMDMs were either infected with *S.* Typhimurium (ST) or pretreated with Concanamycin A (ConcA; 100 nM, 2 h) and then infected with *S.* Typhimurium in the presence of 50 nM Concanamycin A for the indicated time. Total cell lysates were subjected to immunoblot and were stained with an antibody against p62. Concanamycin A inhibits lysosomal acidification of the autophagosome and is used to determine autophagic turnover.

(B) Relative p62 expression levels were determined from three independent immunoblots by densitometric quantification. UI, uninfected. ST, *S.* Typhimurium.

Figures taken from (Hos et al. 2017).

Having shown that p62 markedly accumulates in *Ifnar1-/-* BMDMs, we next analyzed whether elevated p62 levels promote increased survival of *S.* Typhimurium-infected *Ifnar1-/-* BMDMs. For this purpose, WT and *Ifnar1-/-* BMDMs were transfected with control or *Sqstm1*/p62-specific small-interfering RNA (siRNA) and knockdown of p62 was subsequently confirmed by immunoblot (**Fig. 11 A**). Next, p62-dependent macrophage viability was determined 6 h after *S.* Typhimurium infection using a luminescent assay. As expected, survival rates of *Ifnar1-/-* BMDMs transfected with control siRNA, which expressed higher levels of p62, showed significantly increased survival compared to the corresponding WT

BMDMs (**Fig. 11 B**). Importantly, knockdown of p62 significantly reduced cell viability in both WT and *Ifnar1*^{-/-} BMDMs (**Fig. 11 B**) indicating that p62 plays a crucial role in the cell-autonomous defense against *S*. Typhimurium.
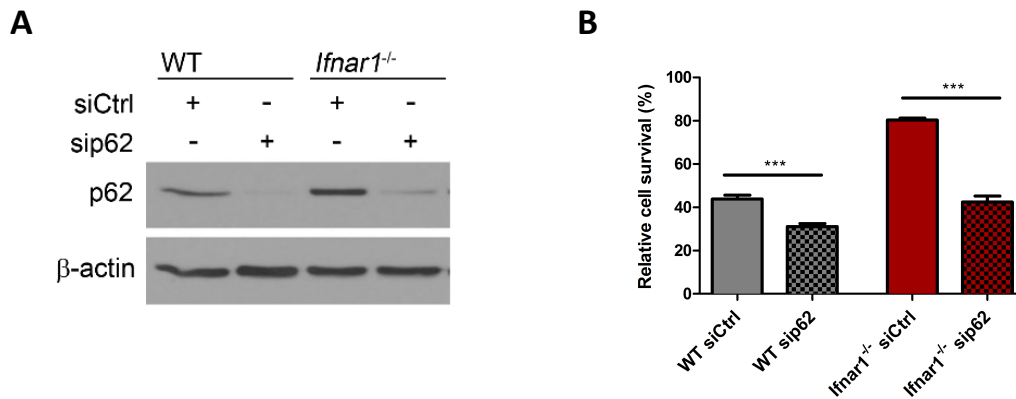

Figure 11. P62 promotes survival of *S*. Typhimurium-infected macrophages.

(A) Immunoblot analysis of p62 knockdown efficiency. WT and *Ifnar1*^{-/-} BMDMs were transfected with non-targeting (siCtrl) or siRNA specific for *Sqstm1/*p62 (sip62). Thereafter, total cell lysates were analyzed for p62 expression by immunoblot.

(B) Luminescence analysis of p62-dependent cell death. Luminescence signals of WT and *Ifnar1*^{-/-} BMDMs transfected with non-targeting (siCtrl) or *Sqstm1/p62*-specific (sip62) siRNA were assessed to determine cell viability 6 h after *S*. Typhimurium infection. Values were normalized to luminescence signal of uninfected WT siCtrl BMDMs.

Figures taken from (Hos et al. 2017).

Since some studies have suggested that autophagy is a critical host defense mechanism against *S*. Typhimurium (Thurston et al. 2009; Zheng et al. 2009), we additionally analyzed cell viability of autophagy-deficient *Atg7*^{-/-} BMDMs upon infection with *S*. Typhimurium. As shown in **Fig. 12**, *Atg7*^{-/-} BMDMs infected with *S*. Typhimurium for 6 h survived even less than WT BMDMs. However, neutralization of IFN-β protected both WT and *Atg7*^{-/-} BMDMs from *S*. Typhimurium-induced cell death (**Fig. 12**). We therefore conclude that IFN-I signaling mediates cell death upon *S*. Typhimurium infection independent of autophagy, but dependent on p62.
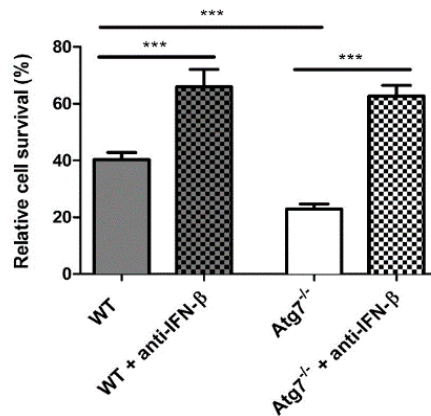
Figure 12. IFN-I signaling mediates cell death of *S*. Typhimurium-infected macrophages independent of autophagy.

Luminescence analysis of autophagy- and IFN-dependent cell death. Autophagy-dependent cell death was determined by measuring the luminescence signals of WT and autophagy-deficient *Atg7*^-/- BMDMS 6 h after *S*. Typhimurium infection. Additionally, IFN-I-dependent cell death was assessed in WT and *Atg7*^-/- BMDMS in the presence of a neutralizing antibody against IFN-β. Values were normalized to luminescence signals of uninfected WT BMDMs treated with an IgG control antibody.

Figure taken from (Hos et al. 2017).

3.6 IFN-I signaling attenuates Nrf2 activation and anti-oxidative responses

Previous work by Komatsu and co-workers as well as by Lau and co-workers has indicated that p62 is of major relevance for regulating anti-oxidative stress response pathways in hepatocytes and epithelial kidney cells, respectively. These authors suggested that high levels of p62 protect cells from pharmacologically induced oxidative damage and cell death. (Komatsu et al. 2010; Lau et al. 2010). Mechanistically, p62 interacts with the Nrf2 binding site on Keap1. As a result of p62-Keap1 interaction, the transcription factor Nrf2 is released from Keap1, stabilized and translocated to the nucleus, where it induces the expression of various detoxifying enzymes and cytoprotective proteins (Ichimura et al. 2013; Komatsu et al. 2010; Lau et al. 2010).

Since p62 strongly accumulated in *S*. Typhimurium-infected *Ifnar1*^-/- BMDMs, we next analyzed whether p62 accumulation correlated with increased Nrf2 activation. As shown in **Fig. 13 A and B**, Nrf2 protein expression of *Ifnar1*^-/- BMDMs was significantly enhanced after 2 h, 4 h and 6 h of *S*. Typhimurium infection compared to WT BMDMs, whereas Keap1 expression was decreased 6 h p.i. (**Fig. 13 C**). Importantly, IFN-I signaling reduced Nrf2 post-

transcriptionally, because mRNA expression was significantly decreased in *S*. Typhimurium-infected *Ifnar1-/-* BMDMs (**Fig. 13 D**).
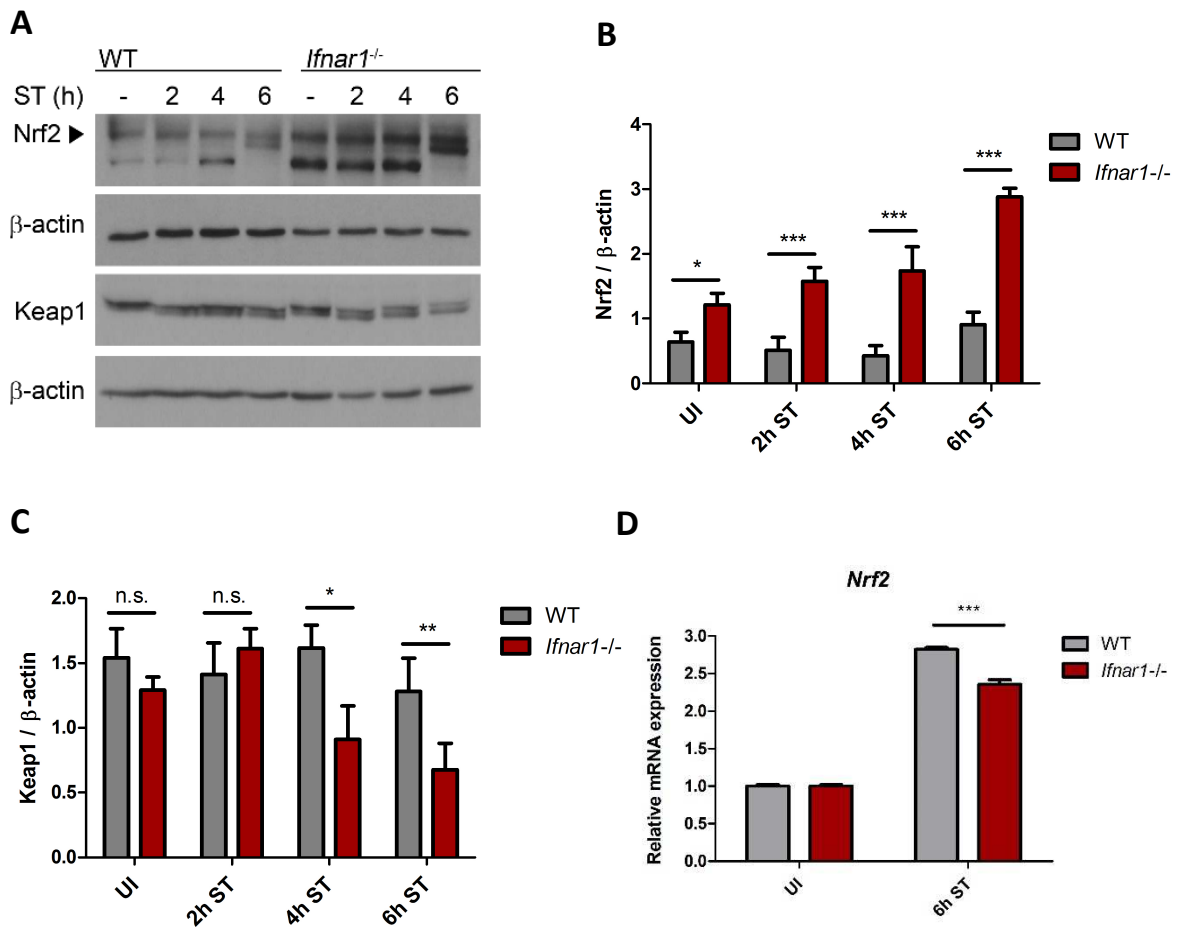
Figure 13. IFN-I signaling decreases Nrf2 protein expression in *S*. Typhimurium-infected macrophages.

(A) Immunoblot analysis of Nrf2 and Keap1. After *S*. Typhimurium (ST) infection for the indicated time points, total cell lysates of WT and *Ifnar1-/-* BMDMs were analyzed for Nrf2 and Keap1 expression by immunoblot.

(B and C) Relative expression of **(B)** Nrf2 and **(C)** Keap1 was determined from three independent immunoblots by densitometric quantification. UI, uninfected. ST, *S*. Typhimurium.

Figures taken from (Hos et al. 2017).

(D) Relative mRNA expression of *Nrf2*. Relative mRNA expression of *Nrf2* in *S*. Typhimurium (ST)-infected WT and *Ifnar1-/-* BMDMs was determined by real-time PCR. Values were normalized to the amounts of mRNA in uninfected (UI) BMDMs.

Using confocal microscopy, we next analyzed p62-Keap1 interaction in infected WT and *Ifnar1-/-* BMDMs stained with antibodies against p62 and Keap1. As shown in **Fig. 14 A and B**, p62 strongly co-localized with Keap1 in infected *Ifnar1-/-* BMDMs. Consistently, we detected significantly more Nrf2 in the nucleus of *Ifnar1-/-* BMDMs compared to WT BMDMs

6 h p.i. (**Fig. 14, C-E**). Furthermore, relative mRNA expression levels of Nrf2 target genes, including *Nqo1, Hmox-1* and *Gclc*, were significantly upregulated in *Ifnar1*$^{-/-}$ BMDMs 2 h and 6 h p.i., respectively, compared to the expression levels in WT BMDMs (**Fig. 14, F-H**).
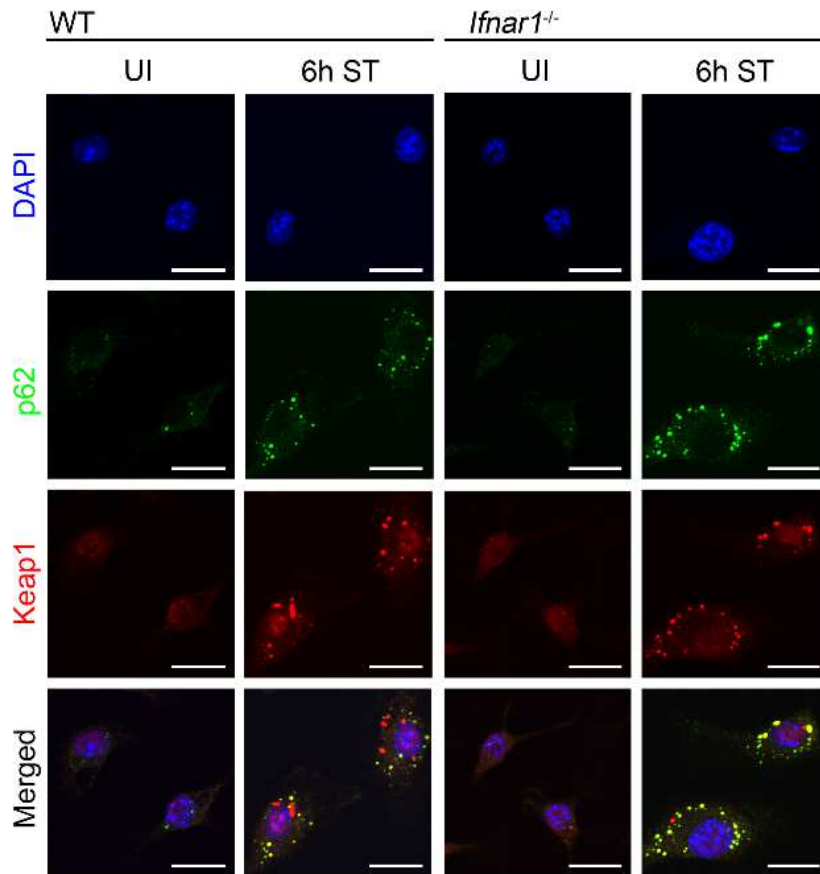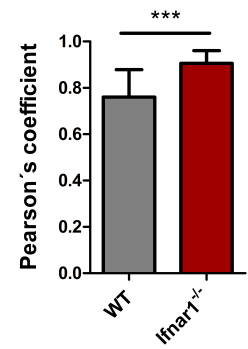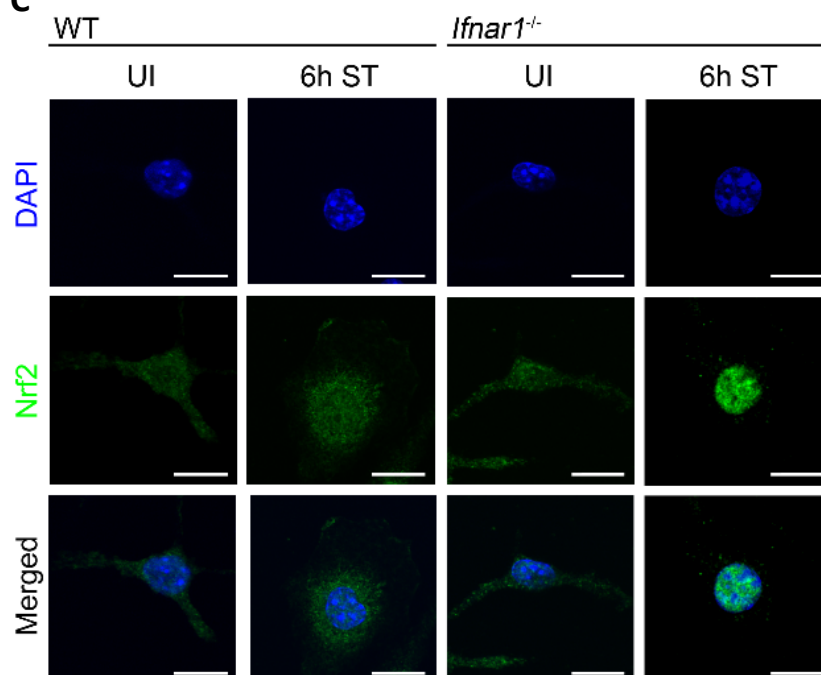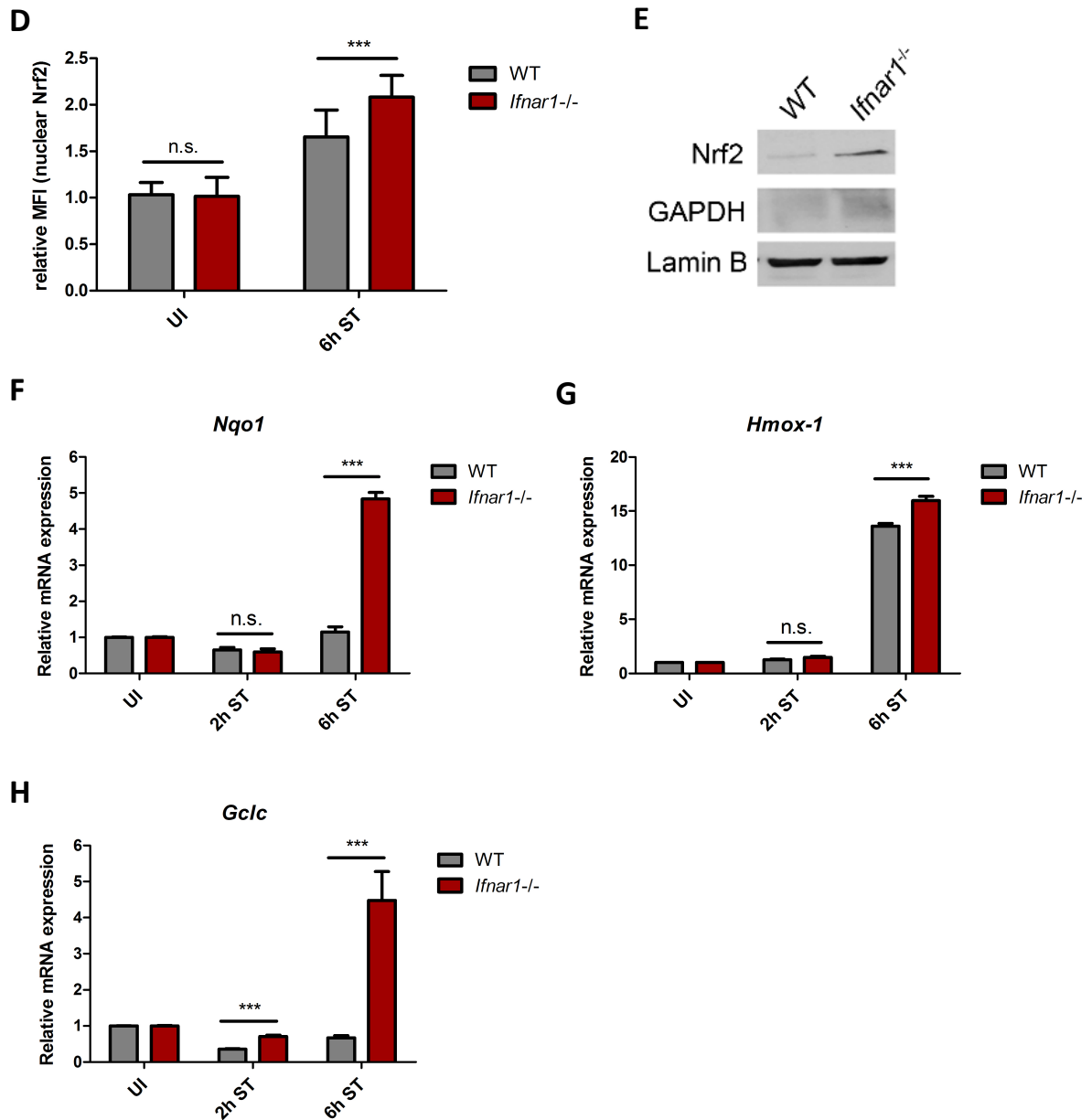
Figure 14. IFN-I signaling attenuates Nrf2 activation and anti-oxidative stress responses in *S.* Typhimurium-infected macrophages.

(A) Immunofluorescence staining of subcellular distribution of p62 and Keap1. WT and *Ifnar1^-/-^* BMDMs were infected with *S.* Typhimurium (ST) for the indicated time and were immunostained for p62 (green) and Keap1 (red), and were examined by confocal microscopy. Scale bars, 10 μm. UI, uninfected.

(B) p62-Keap1 co-localization. Pearson correlation coefficient was used to assess p62 and Keap1 co-localization in WT and *Ifnar1^-/-^* BMDMs 6 h after infection with *S.* Typhimurium.

(C) Immunofluorescence staining of nuclear Nrf2. After 6 h of *S.* Typhimurium (ST) infection, WT and *Ifnar1^-/-^* BMDMs were immunostained for Nrf2 (green) and examined by confocal microscopy. Scale bars, 10 μm. UI, uninfected.

(D) Quantification of nuclear Nrf2. Mean fluorescent intensity (MFI) of nuclear Nrf2 was measured using densitometric quantification (n=50 cells each, repeated for three times). UI, uninfected.

(E) Immunoblot analysis of nuclear Nrf2. Nuclear fractions of WT and *Ifnar1^-/-^* BMDMs were prepared 6 h after *S.* Typhimurium infection and were subjected to immunoblot analysis for Nrf2 expression. Lamin B (nuclear fraction) and GAPDH (cytoplasmic fraction) were used as controls.

(F-H) Relative mRNA expression of Nrf2-dependent genes. Relative mRNA expression levels of **(F)** *Nqo1*, **(G)** *Hmox-1* and **(H)** *Gclc* in *S.* Typhimurium (ST)-infected WT and *Ifnar1*⁻/⁻ BMDMs were determined by real-time PCR. Values were normalized to the amounts of mRNA in uninfected (UI) BMDMs.

Figures taken from (Hos et al. 2017).

To confirm that the upregulation of cytoprotective genes in *Ifnar1*⁻/⁻ BMDMs was mediated by p62, we transfected *Ifnar1*⁻/⁻ BMDMs with control or anti-*Sqstm1/*p62 siRNA (**Fig. 15 A**) and determined relative mRNA expression levels of *Nqo1, Hmox-1* and *Gclc* upon infection with *S.* Typhimurium. As shown in **Fig. 15, B to D**, genetic silencing of *Sqstm1*/p62 significantly reduced *Nqo1, Hmox-1* and *Gclc* expression 6 h p.i. To confirm that p62 accumulation and not autophagy deficiency promotes anti-oxidative responses to *S.* Typhimurium, the expression levels of Nrf2-dependent target genes were additionally assessed in autophagy-deficient *Atg7*⁻/⁻ BMDMs. Autophagy deficiency had no significant effect on Nrf2-dependent gene expression, since expression levels of *Nqo1* and *Gclc* were similar in infected WT and *Atg7*⁻/⁻ BMDMs **(Fig. 15, E and F)**. Neutralization of IFN-β, however, significantly increased mRNA expression of *Nqo1* and *Gclc* in both WT and *Atg7*⁻/⁻ BMDMs (**Fig. 15, E and F**), indicating that p62 expression but not autophagy deficiency is critical for anti-oxidative stress responses to *S.* Typhimurium.

A
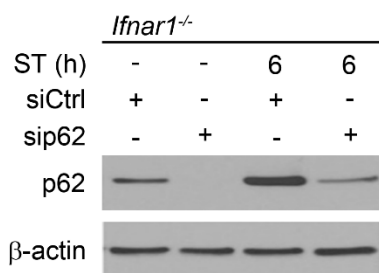
B
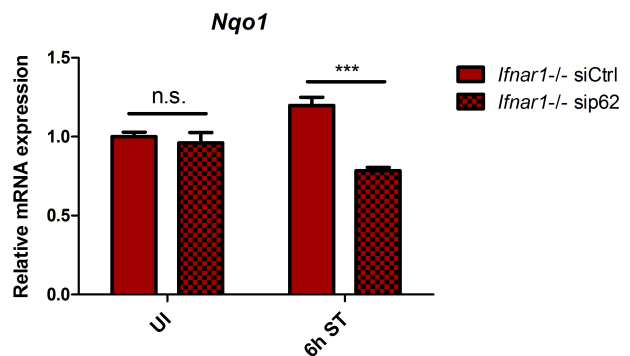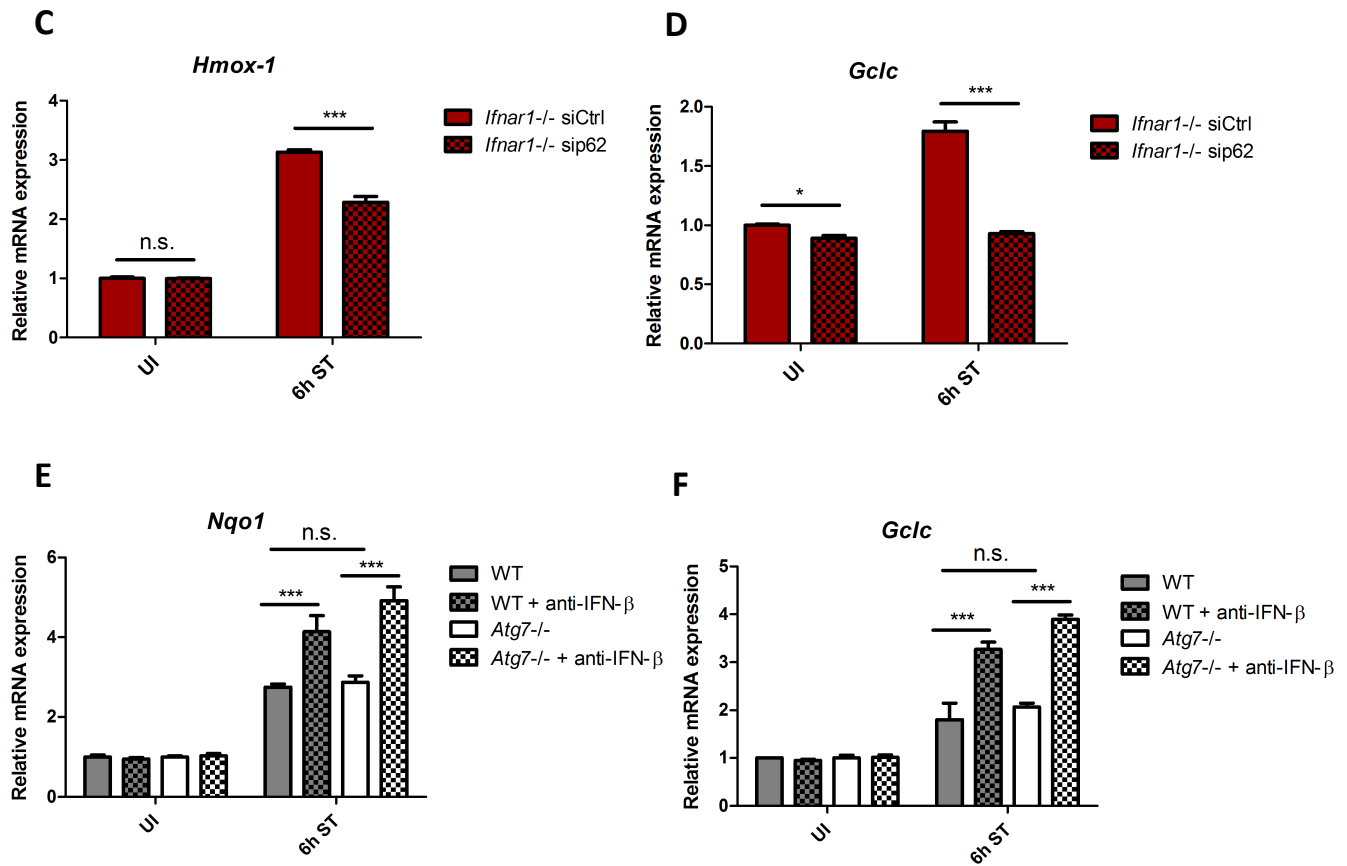
Figure 15. P62 mediates anti-oxidative stress responses to *S*. Typhimurium.

(A) Immunoblot analysis of p62 knockdown efficiency. *Ifnar1*^{-/-} BMDMs were transfected with non-targeting (siCtrl) or siRNA specific for *Sqstm1/*p62 (sip62). Thereafter, total cell lysates were analyzed by immunoblot for p62 expression.

(B-D) P62-dependent mRNA expression of Nrf2 downstream genes. Relative mRNA expression levels of **(B)** *Nqo1*, **(C)** *Hmox-1* and **(D)** *Gclc* in *S*. Typhimurium (ST)-infected *Ifnar1*^{-/-} BMDMs transfected with non-targeting (siCtrl) or siRNA specific for *Sqstm1/*p62 (sip62) were determined by real-time PCR. Values were normalized to the amounts of mRNA in uninfected (UI) siCtrl BMDMs.

(E and F) Autophagy- and IFN-I-dependent expression of Nrf2 downstream genes. WT and *Atg7*^{-/-} BMDMs infected with *S*. Typhimurium (ST) in the presence or absence of a neutralization antibody against IFN-β were assessed for the relative mRNA expression of **(E)** *Nqo1* and **(F)** *Gclc*. Values were normalized to the amounts of mRNA in uninfected (UI) WT BMDMs treated with an IgG control antibody.

Figures taken from (Hos et al. 2017).

Taken together, these results demonstrate that *S*. Typhimurium-induced IFN-I signaling interferes with p62-Keap1 interaction. IFN-I signaling reduces p62 levels in *S*. Typhimurium-infected macrophages, which results in decreased p62-Keap1 interaction eventually leading to impaired Nrf2-dependent cytoprotective gene expression.

3.7 Impaired Nrf2 function mediates *S.* Typhimurium-induced cell death

Having shown that IFN-I signaling reduces Nrf2 activation and the ability to respond to *S.* Typhimurium-induced oxidative stress, we next analyzed whether impaired Nrf2 activation sensitizes macrophages to cell death.

For this purpose, WT and *Ifnar1*$^{-/-}$ BMDMs were transfected with control or *Nfe2l2* (the gene encoding Nrf2)-specific siRNA and cell death upon *S.* Typhimurium infection was assessed using a luminescence assay. Knockdown of Nrf2 was confirmed by immunoblot analysis (**Fig. 16 A**). In line with our previous findings, *S.* Typhimurium infection caused significantly more cell death in WT BMDMs compared to *Ifnar1*$^{-/-}$ BMDMs transfected with control siRNA (**Fig. 16 B**). In WT BMDMs, in which Nrf2 function is already impaired by IFN-I, genetic silencing of *Nrf2* had no additional effect on *S.* Typhimurium-induced cell death. By contrast, Nrf2-deficient *Ifnar1*$^{-/-}$ BMDMs were more susceptible to cell death than *Ifnar1*$^{-/-}$ transfected with control siRNA. In fact, cell death caused by *S.* Typhimurium infection in Nrf2-deficient *Ifnar1*$^{-/-}$ BMDMs was comparable to the amount of cell death in Nrf2-deficient WT BMDMs (**Fig. 16 B**). Hence, Nrf2 critically mediates increased survival of *Ifnar1*$^{-/-}$ BMDMs upon *S.* Typhimurium infection.

To confirm the predominant role of Nrf2 in regulating cell viability, we pharmacologically modified Nrf2 function in WT and *Ifnar1*$^{-/-}$ BMDMs during infection with *S.* Typhimurium. Cell viability was subsequently analyzed 6 h p.i. using a luminescent assay. In line with our Nrf2 knockdown data, pharmacological inhibition of Nrf2 using Trigonelline significantly reduced cell viability in infected *Ifnar1*$^{-/-}$ BMDMs compared to untreated controls, whereas there was only a modest reduction of cell viability in infected WT BMDMs (**Fig. 16 C**). By contrast, pharmacological activation of Nrf2 by CDDO markedly enhanced WT viability following *S.* Typhimurium infection, whereas CDDO had no statistically significant effect on survival of infected *Ifnar1*$^{-/-}$ BMDMs (**Fig. 16 C**), in which Nrf2 function is already highly upregulated.
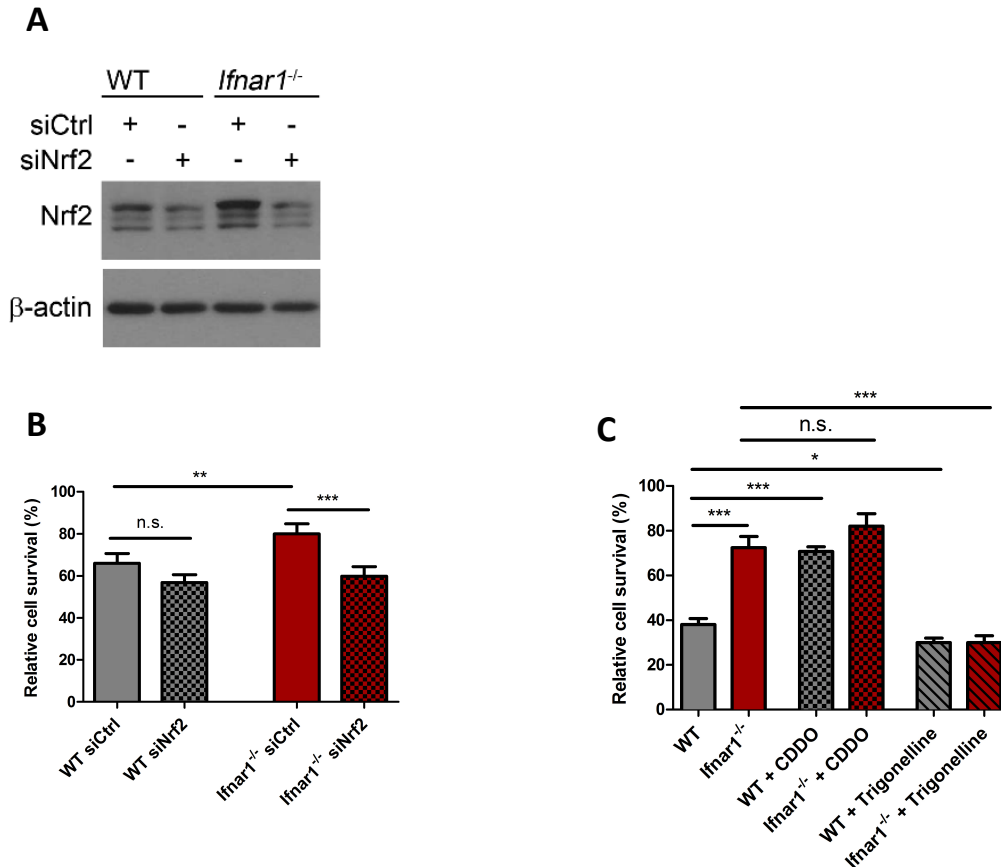
Figure 16. IFN-I signaling induces cell death through impairing Nrf2.

(A) Immunoblot analysis of Nrf2 knockdown efficiency. WT and *Ifnar1*−/− BMDMs were transfected with non-targeting (siCtrl) or siRNA specific for *Nfe2l2* (siNrf2). Thereafter, total cell lysates were analyzed by Western blot for Nrf2.
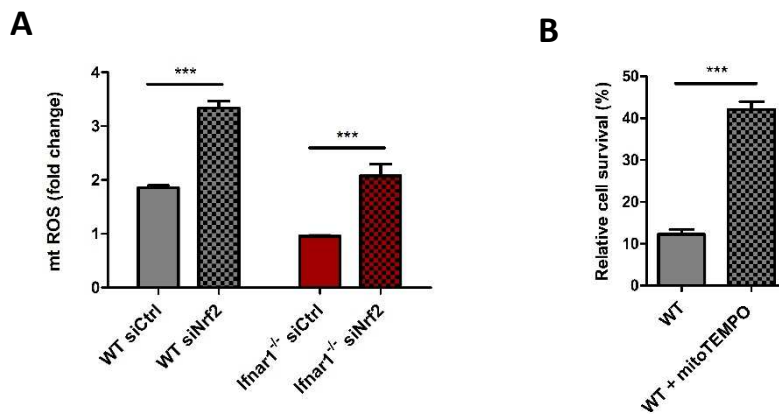
(B) Luminescence analysis of Nrf2-dependent cell death. Luminescence signals of WT and *Ifnar1*−/− BMDMs transfected with non-targeting (siCtrl) or siRNA specific for *Nfe2l2* (siNrf2) were assessed to determine cell viability upon infection with *S.* Typhimurium (6 h p.i.). Values were normalized to luminescence signal of uninfected WT BMDMs.

(C) Luminescence analysis of cell death upon pharmacological modulation of Nrf2 activation. Luminescence signals of WT and *Ifnar1*−/− BMDMs treated with the Nrf2 activator CDDO (500 nM, 6 h) or with the Nrf2 inhibitor Trigonelline (100 µM, 6 h) were determined to analyze cell viability 6 h after *S.* Typhimurium infection. Values were normalized to luminescence signal of uninfected, untreated WT BMDMs.

Figures taken from (Hos et al. 2017).

Having demonstrated that *S.* Typhimurium infection induces mtROS in macrophages (**Fig. 4 A**), we next assessed whether mtROS production was dependent on Nrf2 activation. For this purpose, WT and *Ifnar1*−/− BMDMs were infected with *S.* Typhimurium for 6 h and mitochondrial ROS was quantified using MitoSOX staining upon knockdown of Nrf2. As shown in **Fig. 17 A**, knockdown of Nrf2 significantly enhanced mitochondrial ROS production

in WT and *Ifnar1*^{-/-} BMDMs compared to controls. As we observed that WT BMDMs were more susceptible to *S.* Typhimurium-induced cell death because of impaired Nrf2 function and reduced anti-oxidative stress responses, we surmised that scavenging mitochondrial ROS might be cytoprotective. Therefore, we specifically quenched mitochondrial ROS in *S.* Typhimurium-infected WT BMDMs using mitoTEMPO. In fact, quenching mitochondrial ROS significantly improved WT survival compared to untreated controls (**Fig. 17 B**), indicating that disturbed redox homeostasis caused by *S.* Typhimurium infection is an important trigger for cell death.

Figure 17. Impaired Nrf2 function causes cell death through mitochondrial ROS.

(A) Nrf2-dependent mitochondrial reactive oxygen species (mtROS) production. WT and *Ifnar1*^{-/-} BMDMs were transfected with non-targeting (siCtrl) or siRNA specific for *Nfe2l2* (siNrf2). Transfected BMDMs were infected with *S.* Typhimurium for 6 h and the amounts of mtROS relative to uninfected WT siCtrl BMDMs were analyzed by FACS using MitoSOX staining.

(B) Luminescence analysis of ROS-dependent cell death. Luminescence signals of WT BMDMs treated with or without the mtROS scavenger mitoTEMPO (100 µM, 6 h) were analyzed to determine cell viability upon *S.* Typhimurium (ST) infection (6 h p.i.). Values were normalized to luminescence signal of uninfected, untreated WT BMDMs.

Figures taken from (Hos et al. 2017).

Collectively, these results demonstrate that *S.* Typhimurium-induced IFN-I impairs Nrf2 activation, which leads to increased mitochondrial ROS production eventually sensitizing infected macrophages to cell death.

3.8 Nrf2 function is regulated by RIP3

We have recently shown that *S.* Typhimurium exploits the host`s IFN-I response to induce RIP1- and RIP3-mediated necroptosis in macrophages (Robinson et al. 2012). As RIP kinases act downstream of the IFN-I receptor, we speculated that IFN-I regulates Nrf2 function through RIP signaling.

As shown in **Fig. 18 A**, *S.* Typhimurium infection lead to the activation of necroptosis pathways indicated by phosphorylation of RIP3 2 h and 6 h p.i., which was mediated by IFN-I signaling. Accordingly, *S.* Typhimurium infection promoted the phosphorylation of MLKL (**Fig. 18 A**), a downstream target of RIP3, which was remarkably reduced in infected *Ifnar1*⁻/⁻ (**Fig. 18 A**) and *RIP3*⁻/⁻ BMDMs (**Fig. 18 B**). As *S.* Typhimurium infection induced more IL-1β expression in *Ifnar1*⁻/⁻ BMDMs compared to WT BMDMs, we excluded pyroptosis as the predominant type of cell death mediated by IFN-I signaling (**Fig. 18, C and D**). Similar to *Ifnar1*⁻/⁻ BMDMs, *S.* Typhimurium-infected *RIP3*⁻/⁻ BMDMs showed accumulation of p62, reduced Keap1 and increased Nrf2 expression compared to infected WT BMDMs (**Fig. 18 E**).
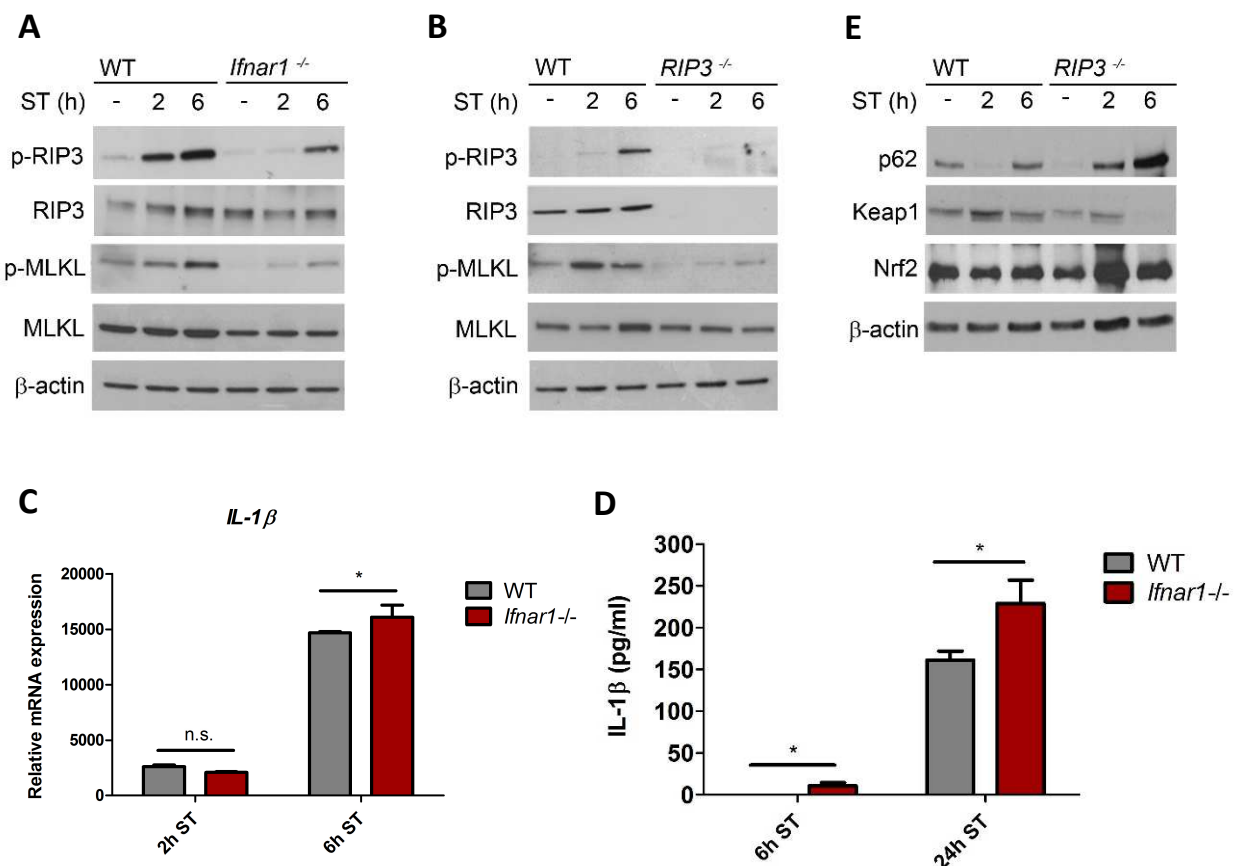
Figure 18. *S*. Typhimurium infection activates RIP3 downstream of Ifnar1.

(A and B) Immunoblot analysis of RIP3 and MLKL activation. After *S*. Typhimurium (ST) infection for the indicated time, total cell lysates of **(A)** WT and *Ifnar1^-/-^* or **(B)** WT and *RIP3^-/-^* BMDMs, respectively, were subjected to immunoblot analysis and were stained with antibodies against RIP3, phsopho-RIP3 (p-RIP3), MLKL and phospho-MLKL (p-MLKL) as markers for necroptotic pathway activation.

(C) Relative *IL-1β* mRNA expression. WT and *Ifnar1^-/-^* BMDMs were infected with *S*. Typhimurium (ST) for 6 h and relative *IL-1β* mRNA expression was determined by real-time PCR. Values were normalized to the amounts of mRNA of uninfected (UI) BMDMs.

(D) Analysis of IL-1β secretion. Supernatants of WT and *Ifnar1^-/-^* BMDMs infected with *S*. Typhimurium (ST) for 6 h and 24 h, respectively, were collected and analyzed for IL-1 β secretion by ELISA.

(E) Immunoblot analysis of p62, Keap1 and Nrf2. Expression levels of p62, Keap1 and Nrf2 were analyzed by immunoblot in total cell lysates of *S*. Typhimurium (ST)-infected WT and *RIP3^-/-^* BMDMs at the indicated time points.

Figures taken from (Hos et al. 2017).

We additionally assessed nuclear translocation of Nrf2 by confocal microscopy and found that loss of RIP3 facilitated nuclear translocation of Nrf2 6 h after *S*. Typhimurium infection (**Fig. 19 A**). Additionally, we detected more Nrf2 in the nuclear fractions of infected *RIP3^-/-^* BMDMs compared to WT BMDMs (**Fig. 19 B**). Enhanced nuclear localization of Nrf2 in *RIP3^-/-^* BMDMs resulted in significantly upregulated *Nqo1* and *Gclc* mRNA expression 6 h p.i. (**Fig. 19, C and D**).
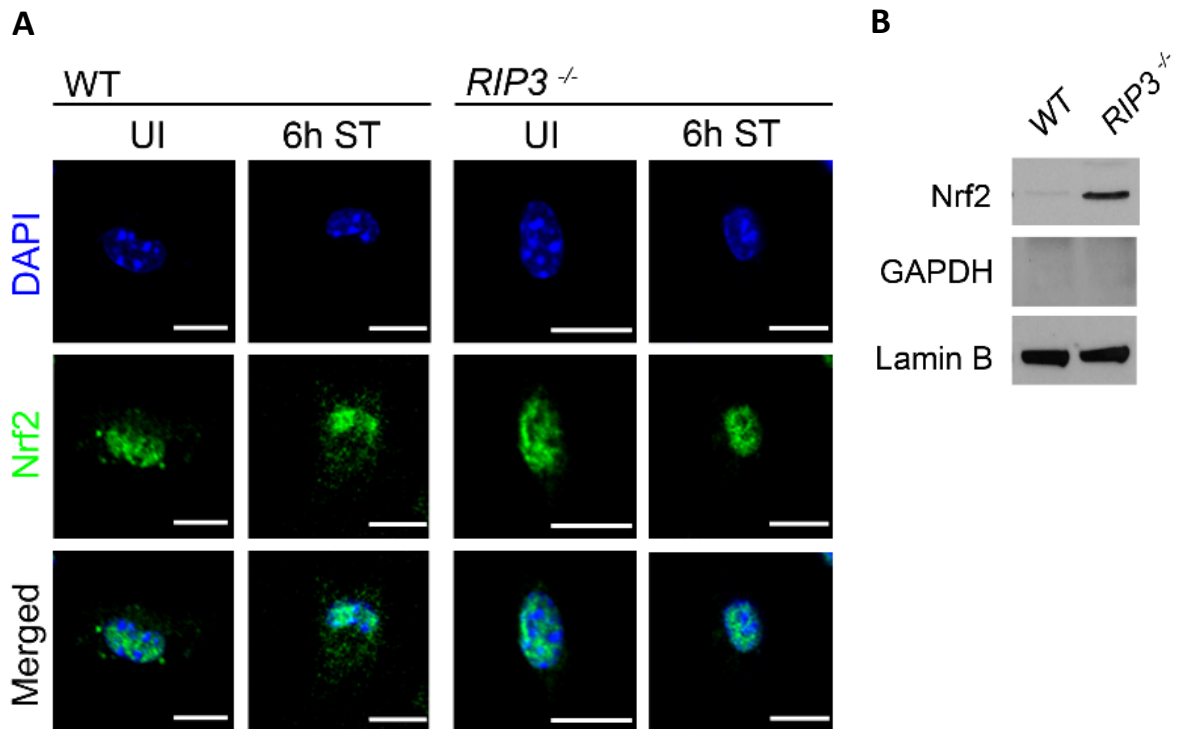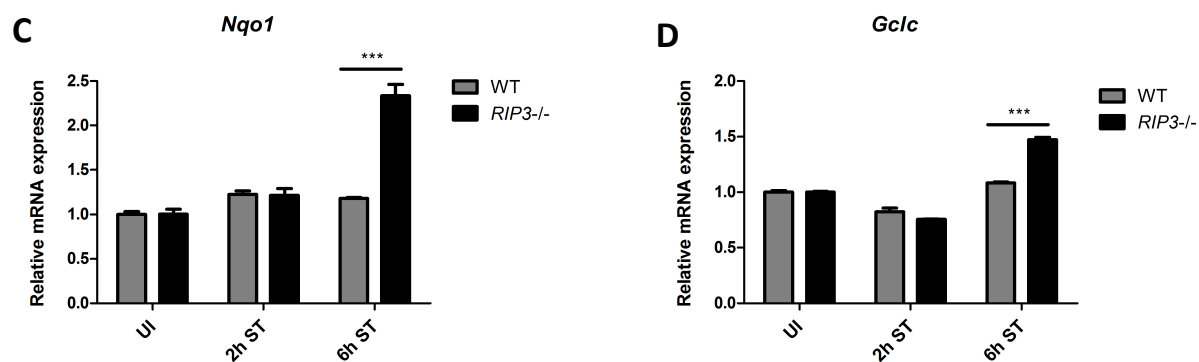
Figure 19. RIP3 impairs Nrf2 function in *S*. Typhimurium-infected macrophages.

(A) Immunofluorescence staining of nuclear Nrf2. After 6 h of *S*. Typhimurium (ST) infection, WT and *RIP3^-/-*^ BMDMs were immunostained for Nrf2 (green) and subcellular localization of Nrf2 was examined by confocal microscopy. Scale bars, 10 μm. UI, uninfected.

(B) Immunoblot analysis of nuclear Nrf2. Nuclear fractions of WT and *RIP3^-/-^* BMDMs were prepared 6 h after *S*. Typhimurium infection and were subjected to immunoblot analysis for Nrf2 expression. Lamin B (nuclear fraction) and GAPDH (cytoplasmic fraction) were used as controls.

(C and D) RIP3-dependent expression of Nrf2 target genes. Relative mRNA expression levels of **(C)** *Nqo1* and **(D)** *Gclc* in *S*. Typhimurium (ST)-infected WT and *RIP3^-/-^* BMDMs were determined by real-time PCR. Values were normalized to the amounts of mRNA of uninfected (UI) BMDMs.

Figures taken from (Hos et al. 2017).

These results collectively indicate that IFN-I signaling activates RIP3, which interferes with Nrf2 function resulting in an impaired anti-oxidative response to *S*. Typhimurium infection.

3.9   Pgam5 prevents Nrf2 activation downstream of IFN-I/RIP3

We next sought to identify the mechanism by which IFN-I/RIP3 signaling impairs Nrf2 function. Wang and co-workers have reported previously that MLKL mediates the interaction of RIP1- and RIP3-containing protein complexes with the mitochondrial phosphatase Pgam5 upon TNF-induced necrosis (Wang et al. 2012). Pgam5 is subsequently recruited to the outer mitochondrial membrane, where it forms a ternary complex with Nrf2 and Keap1, in which Keap1 bridges Pgam5 and Nrf2 (Lo and Hannink 2008). We therefore investigated whether

IFN-I/RIP3 signaling regulates Pgam5 expression upon *S.* Typhimurium infection of macrophages and whether Pgam5 affects Nrf2 activation.

As shown in **Fig. 20 A and B**, *S.* Typhimurium infection induced the expression of Pgam5 in WT, *Ifnar1*^{-/-} and *RIP3*^{-/-} BMDMs 2 h and 6 h p.i., respectively. However, loss of either IFN-I or RIP3 markedly reduced Pgam5 expression (**Fig. 20, A and B**). To investigate whether Pgam5 interacts with Nrf2, anti-Nrf2 immunoprecipitates of WT, *Ifnar1*^{-/-} and *RIP3*^{-/-} BMDMs were analyzed by immunoblot. Pgam5 strongly co-immunoprecipated with Nrf2 in WT BMDMs 6 h after *S.* Typhimurium infection, whereas Pgam5 was not detectable in anti-Nrf2 immunoprecipitates of *Ifnar1*^{-/-} and *RIP3*^{-/-} BMDMs (**Fig. 20, C and D**). This finding therefore indicates that *S.* Typhimurium-induced IFN-I/RIP3 signaling promotes the formation of a protein complex comprising Pgam5 and Nrf2.

D
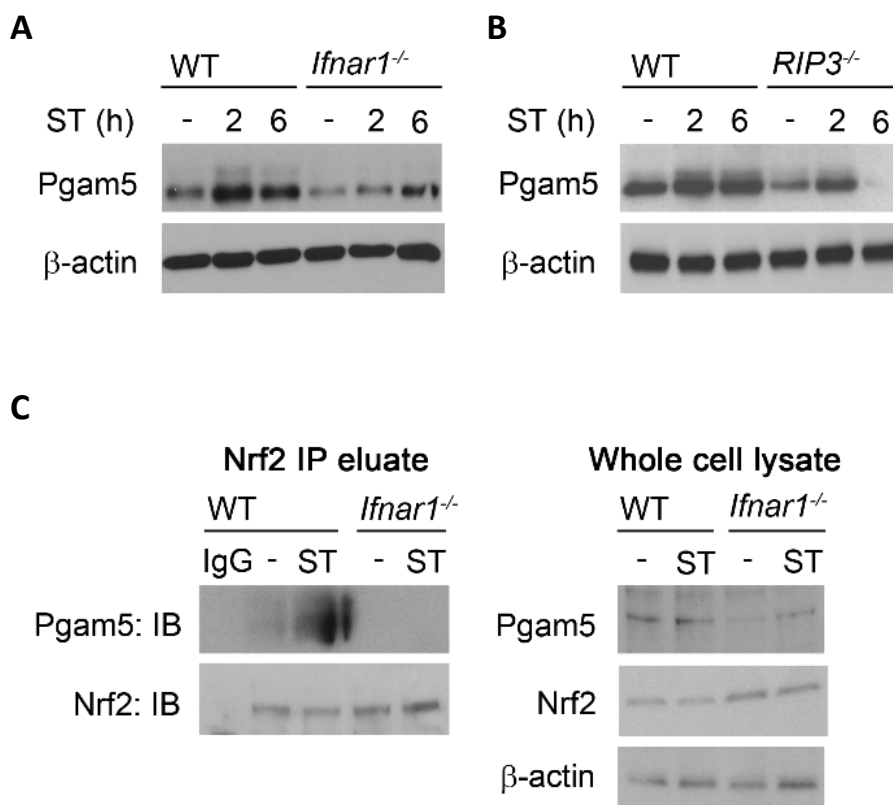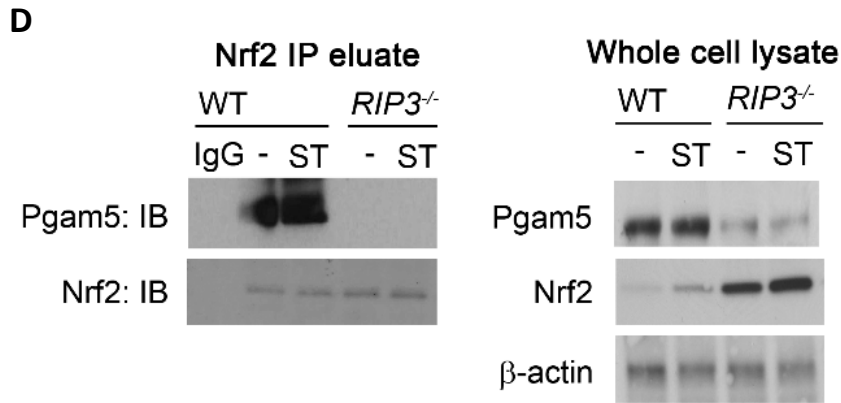
Figure 20. IFN-I/RIP3 signaling promotes the interaction of Pgam5 with Nrf2.

(A and B) Immunoblot analysis of Pgam5. At the indicated time points, total cell lysates of *S.* Typhimurium (ST)-infected **(A)** WT and *Ifnar1⁻/⁻* BMDMs or **(B)** WT and *RIP3⁻/⁻* BMDMs were subjected to immunoblot and were analyzed for Pgam5 expression.

(C and D) Immunoprecipitation analyses. Anti-Nrf2 immunoprecipitates (IP) and whole cell lysates from **(C)** WT and *Ifnar1⁻/⁻* BMDMs or **(D)** WT and *RIP3⁻/⁻* BMDMs infected with *S.* Typhimurium (ST) for 6 h were analyzed by immunoblot (IB) with antibodies against Pgam5 and Nrf2. Samples treated with non-specific IgG were used as controls.

Figures taken from (Hos et al. 2017).

As Pgam5 interacts with Nrf2, we next sought to investigate whether Pgam5 regulates Nrf2 function. For this purpose, WT BMDMs were transfected with either control or *Pgam5*-specific siRNA and knockdown of Pgam5 was confirmed by immunoblot (**Fig. 21 A**). Using confocal microscopy, we found that genetic silencing of Pgam5 enhanced nuclear translocation of Nrf2 6 h after infection with *S.* Typhimurium compared to WT controls (**Fig. 21 B**), which resulted in the enhanced transcription of Nrf2-dependent *Nqo1* (**Fig. 21 C**).

B
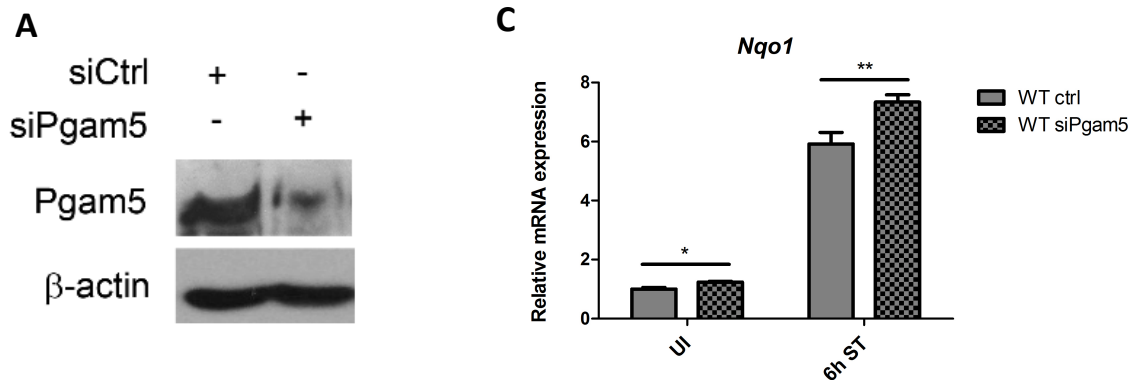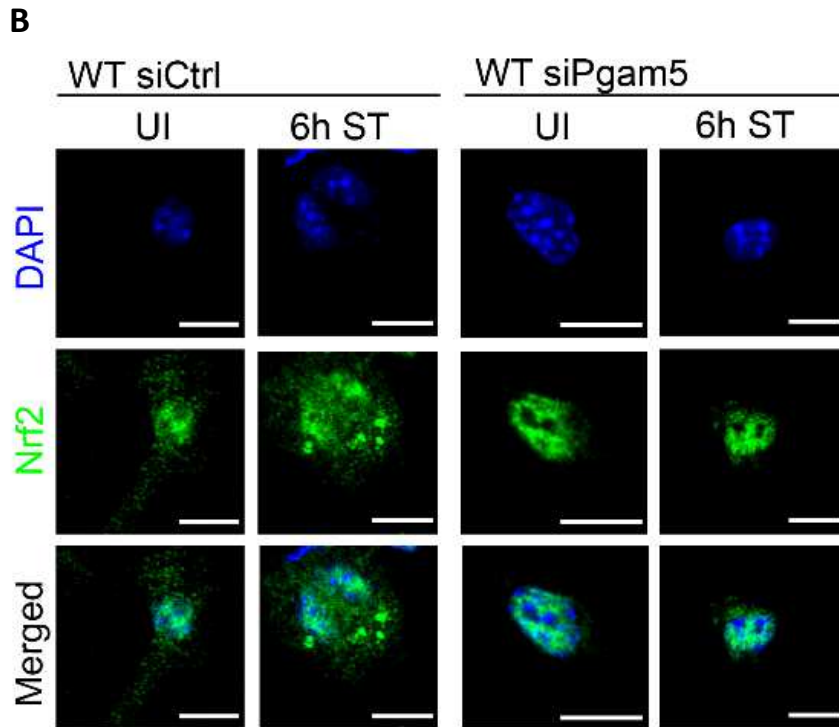
Figure 21. Pgam5 prevents Nrf2 activation downstream of IFN-I/RIP3.

(A) Immunoblot analysis of Pgam5 knockdown efficiency. WT BMDMs were transfected with non-targeting (siCtrl) or *Pgam5*-specific siRNA (siPgam5). Thereafter, Pgam5 knockdown efficiency was determined in total cell lysates by immunoblotting.

(B) Immunofluorescence staining of nuclear Nrf2. WT BMDMs were transfected with non-targeting (siCtrl) or *Pgam5*-specific siRNA (siPgam5). After 6 h of *S.* Typhimurium (ST) infection, transfected BMDMs were immunostained for Nrf2 (green) and subcellular localization of Nrf2 was examined by confocal microscopy. Scale bars, 10 μm. UI, uninfected.

(C) Pgam5-dependent *Nqo1* mRNA expression. WT BMDMs were transfected with non-targeting (siCtrl) or *Pgam5*-specific siRNA (siPgam5) and infected with *S.* Typhimurium (ST) for 6 h. Relative mRNA expression of *Nqo1* was subsequently determined by real-time PCR. Values were normalized to the amounts of mRNA in uninfected (UI) WT siCtrl BMDMs.

Figures taken from (Hos et al. 2017).

In summary, these results indicate that *S.* Typhimurium infection enhances the interaction of Pgam5 with Nrf2 through activation of IFN-I and RIP3 signaling pathways. Enhanced Pgam5-Nrf2 interaction eventually impairs Nrf2 function and Nrf2-dependent redox homeostasis of *S.* Typhimurium-infected macrophages.

4. DISCUSSION

An important virulence strategy of *S.* Typhimurium is the induction of cell death within cells of the innate immune system. This enables *S.* Typhimurium to evade the host´s innate immune response and to promote its own pathogenicity. Our previous results have demonstrated that *S.* Typhimurium exploits the host´s IFN-I response to promote RIP3-dependent necroptosis in macrophages. Therefore, macrophages that lack the receptor for IFN-I (*Ifnar1*$^{-/-}$) were less susceptible to *S.* Typhimurium-induced cell death than wildtype macrophages (Robinson et al. 2012). Importantly, macrophages subjected to IFN-I treatment without infection do not undergo cell death, indicating that during *S.* Typhimurium infection additional events combined with IFN-I signaling cumulate in necroptosis.

Here, we investigated the IFN-I-mediated events that lead to necroptosis execution in *S.* Typhimurium-infected macrophages. We found that IFN-I signaling impairs Nrf2-dependent anti-oxidative stress responses to *S.* Typhimurium infection, which results in ROS-mediated mitochondrial dysfunction and subsequent cell death. We specifically show that *S.* Typhimurium-induced IFN-I activates RIP3, which promotes the expression of the mitochondrial phosphatase Pgam5 and its complex formation with Nrf2. Enhanced Pgam5-Nrf2 interaction attenuates nuclear translocation of Nrf2 and the transcription of Nrf2-dependent anti-oxidative genes. The impaired ability of macrophages to respond to *S.* Typhimurium-induced oxidative stress leads to ROS-mediated mitochondrial damage and energy depletion, which transiently triggers autophagy and reduces p62 levels. IFN-I perturbs the interaction of p62 with Keap1 thereby further downregulating Nrf2-dependent anti-oxidative genes eventually sensitizing infected macrophages to cell death (**Fig. 22**).
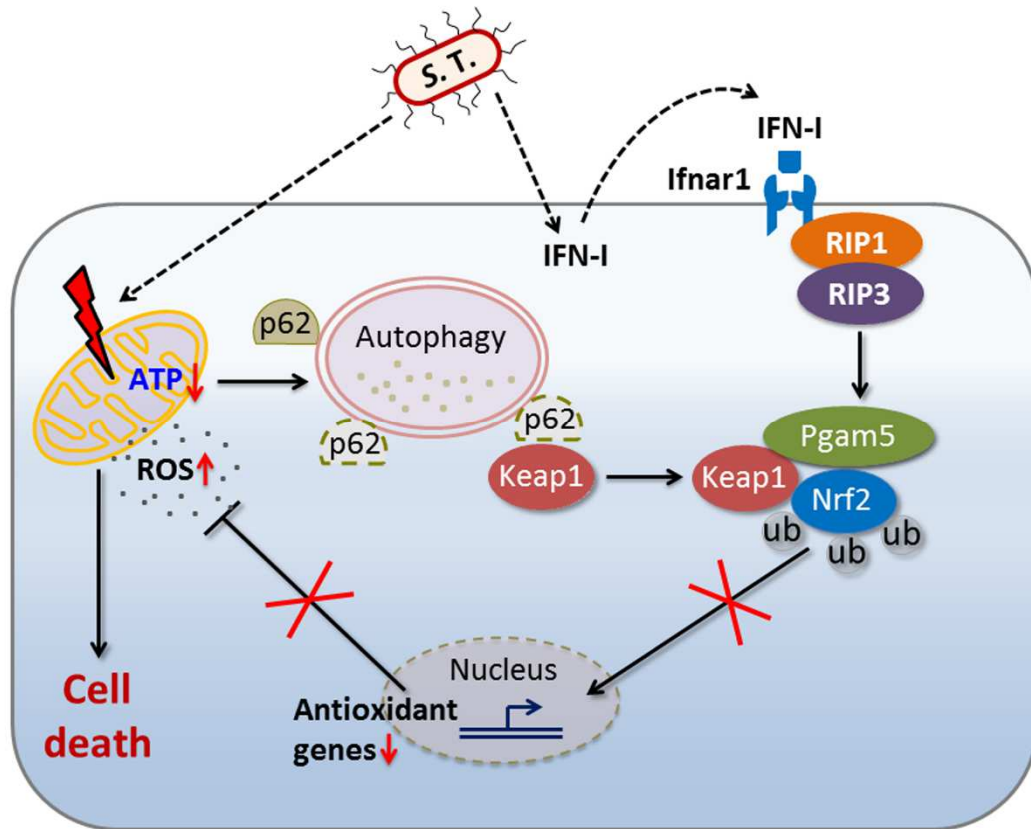
Figure 22. IFN-I signaling exacerbates mitochondrial damage and cell death by preventing Nrf2-dependent antioxidant response.

S. Typhimurium infection induces the para- and autocrine secretion of type I interferon (IFN-I), which subsequently binds to the IFN-I receptor (Ifnar1). In *S.* Typhimurium (S.T.)-infected macrophages, IFN-I induces RIP3-mediated Pgam5 expression. Pgam5 subsequently interacts with Nrf2 (presumably through Keap1), which sequesters Nrf2 in the cytosol thereby repressing the transcription of Nrf2-dependent anti-oxidative genes. *S.* Typhimurium-induced oxidative damage results in ROS-mediated mitochondrial dysfunction, energy depletion, transient induction of autophagy and autophagic degradation of p62. Reduced p62 levels impair interaction of p62 with Keap1, which further decreases Nrf2-dependent anti-oxidative responses to *S.* Typhimurium infection and sensitizes infected macrophages to cell death.

Figure taken from (Hos et al. 2017).

4.1. IFN-I signaling exacerbates *S.* Typhimurium-induced mitochondrial dysfunction and oxidative stress

Mitochondria are key organelles, which provide most of the cellular ATP, but have also been recognized as important mediators of innate immune signaling and programmed cell death (Chandel 2014; Wasilewski and Scorrano 2009; Weinberg et al. 2015). Therefore, disruption of mitochondrial integrity has been identified as a key virulence strategy of both viral and bacterial pathogens (Arnoult et al. 2009; Stavru et al. 2011). Here, we demonstrate

that *S.* Typhimurium infection causes mitochondrial damage in macrophages, which leads to mitochondrial ROS production and decreased ATP levels. In line with our findings, Hernandez and co-workers reported that *S.* Typhimurium disrupted mitochondrial function in a virulence-dependent manner. Upon *S.* Typhimurium infection of macrophages, the SPI-1-encoded effector protein SipB translocated to mitochondria, which appeared swollen and devoid of christae, resulting in macrophage death (Hernandez et al. 2003).

Although we did not specifically investigate virulence-dependent mechanisms of mitochondrial damage, we found that the host´s IFN-I response further exacerbated mitochondrial dysfunction. Our results indicate that IFN-I signaling during *S.* Typhimurium infection of macrophages further enhances mitochondrial ROS production and decreases cellular ATP levels due to the activation of RIP3, which represses the transcription of Nrf2-dependent anti-oxidative enzymes. Although it is well accepted that mitochondrial DNA can engage the cGAS-STING cytosolic DNA sensing machinery to trigger IFN-I production (Li and Chen 2018), very little is known on how IFN-I signaling in turn regulates mitochondrial function. In a previous study by Lewis and co-workers IFN-I treatment of murine L929 and human Daudi lymphoblastoid cells decreased the expression of mitochondrial genes and cellular ATP levels. These authors concluded that functional impairment of the mitochondrial electron transport chain was responsible for the anti-proliferative effect mediated by IFN-I (Lewis et al. 1996). Although we cannot rule out that IFN-I signaling directly causes mitochondrial damage, our present results indicate that IFN-I signaling rather interferes with the expression of Nrf2-dependent detoxifying and protective enzymes thereby indirectly exacerbating *S.* Typhimurium-induced mitochondrial damage.

4.2. IFN-I signaling transiently triggers autophagy

A decrease in cellular ATP leads to the activation of autophagy to maintain energy homeostasis (Mihaylova and Shaw 2011). In line with this notion, our results also demonstrate that *S.* Typhimurium infection transiently triggers autophagy in macrophages because of reduced ATP levels. By contrast, autophagy is triggered to a much lower extend in the

absence of IFN-I signaling, where ATP levels remain higher. Accordingly, recent work has shown that IFN-I treatment induced autophagy in multiple cancer cell lines. This effect was mediated by inhibition of mTORC1, a master regulator of autophagy (Schmeisser et al. 2013). In our study, however, autophagy is induced independent of mTORC1 inhibition, as mTORC1 is activated shortly after *S.* Typhimurium infection. Furthermore, our results demonstrate that mTORC1 activation during S. Typhimurium infection occurs independent of IFN-I signaling.

Likewise, a study by Owen and colleagues reported that mTORC1 was activated upon *S.* Typhimurium infection resulting in the blockade of autophagy (Owen et al. 2014). In line with this observation, we also found that autophagy is blocked at later stages of infection and that loss of IFN-I signaling further attenuates autophagy. Furthermore, recent studies have shown that *S.* Typhimurium was degraded along with autophagic cargo resulting in the enzymatic degradation of bacteria (Birmingham et al. 2006; Zheng et al. 2009). Blockade of autophagy could therefore be a strategy used by *S.* Typhimurium to prevent autophagic degradation. However, our results do not support this notion as bacterial numbers do not differ between WT macrophages, which show higher autophagic activity, compared to *Ifnar1*^{-/-} macrophages, in which autophagic flux was reduced. Accordingly, previous work from our group demonstrated that *S.* Typhimurium co-localized with LC3-positive structures only after one hour of infection, whereas *S.* Typhimurium escaped from these structures after four hours of infection (Ganesan et al. 2017).

We have recently demonstrated that reduction of cellular ATP levels during *S.* Typhimurium infection resulted in activation of the cytoplasmic energy sensor AMPK, an important checkpoint of mTORC1 and autophagy. We found that *S.* Typhimurium targeted AMPK for lysosomal degradation in a SPI-2-dependent manner leading to the inhibition of autophagy and loss of energy (Ganesan et al. 2017). In addition, work from our group revealed that *S.* Typhimurium impairs glycolytic pathways thereby further limiting cellular energy resources (Gutiérrez et al., unpublished data). We therefore conclude that interfering

with cellular energy homeostasis is a key virulence strategy employed by *S*. Typhimurium to impair cell autonomous defense mechanisms and to promote its own intracellular survival.

4.3   IFN-I signaling reduces p62 levels through autophagic degradation

Inhibition of autophagy leads to the accumulation of p62-positive protein aggregates and cytosolic inclusion bodies, which is relevant to human disease (Komatsu et al. 2007; Zatloukal et al. 2002). For instance, p62-positive protein aggregates have been shown to play an important role in neurodegenerative disorders, such as Parkinson´s and Alzheimer´s disease (Hara et al. 2006; Komatsu et al. 2006; Rubinsztein 2006), chronic liver inflammation (Denk et al. 2006; Stumptner et al. 2007), and various cancer entities (Inami et al. 2011; Mathew et al. 2009; Thompson et al. 2003; Umemura et al. 2016). In this study, we found that p62 expression is also increased, both on mRNA and protein levels, upon *S*. Typhimurium infection of macrophages. Furthermore, we observed the formation of p62-containing protein aggregates in the perinuclear region of infected macrophages. Of note, IFN-I signaling reduces the number of p62-positive punctae through increased autophagolysosomal degradation of p62. Our finding that IFN-I signaling reduces p62 levels is supported by a recent study from Ejlerskov and colleagues, who also observed a strong accumulation of p62 in IFN-β-deficient neuronal cells (Ejlerskov et al. 2015).

While high p62 levels have mainly been considered as harmful upon chronic diseases, we found that accumulation of p62 in *Ifnar1*^{-/-} macrophages is protective upon acute infection with *S*. Typhimurium. Our present results indicate that high p62 levels critically mediate survival of *S*. Typhimurium-infected macrophages, since knockdown of *Sqstm1*/p62 significantly decreases macrophage viability. Similarly, p62 has previously been shown to mediate macrophage survival after pharmacological activation of the NLRP3 inflammasome (Zhong et al. 2016). In that study, p62 promoted clearance of damaged mitochondria through Parkin-mediated mitophagy thereby reducing mitochondrial ROS production and anti-oxidative stress. Importantly, we also found that high p62 levels reduce *S*. Typhimurium-

induced anti-oxidative stress through the increased transcription of Nrf2-dependent anti-oxidative genes.

4.4. IFN-I signaling disrupts Nrf2-dependent anti-oxidative stress responses

Beyond its function as an autophagic adaptor protein, p62 also plays an important role in regulating cellular redox homeostasis via its interference with the Nrf2-Keap1 pathway. The Nrf2-Keap1 pathway is a major regulator of anti-oxidative stress responses, and p62 is known to activate this pathway by suppressing Keap1-Nrf2 interaction in the cytosol. In the presence of high p62 levels, Keap1 displays higher binding affinity for p62 than for Nrf2 (Ichimura et al. 2013). Hence, the transcription factor Nrf2 is released from Keap1, stabilized and translocated to the nucleus, where it induces the transcription of several anti-oxidative enzymes, such as *Hmox-1*, *Nqo1* and *Gclc*, promoting cellular survival (Ichimura et al. 2013; Komatsu et al. 2010; Lau et al. 2010). The p62-Nrf2-Keap1 pathway has mainly been studied in the context of cancer pathogenesis, where high Nrf2 activity has been associated with poor prognosis as cancer cells were more resistant to chemotherapy induced anti-oxidative stress (Jaramillo and Zhang 2013; Umemura et al. 2016).

Here, we demonstrate that the p62-Nrf2-Keap1 pathway is also important for cell autonomous immune defenses against *S.* Typhimurium and that the host´s IFN-I response negatively regulates this pathway by decreasing p62 levels. We found that IFN-I signaling reduces the expression and nuclear translocation of Nrf2 in *S.* Typhimurium-infected macrophages, which impairs the transcription of the Nrf2-dependent anti-oxidative enzymes *Hmox-1*, *Nqo1* and *Gclc*. Our results indicate that IFN-I signaling mediates Nrf2 degradation (presumably through the proteasomal pathway) rather than reducing *Nrf2* transcription as IFN-I signaling increases mRNA expression of *Nrf2* in *S.* Typhimurium-infected macrophages. Our observation that Nrf2 expression is regulated post-transcriptionally is in agreement with previous findings demonstrating that Keap1 mediated the ubiquitination and subsequent proteasomal degradation of Nrf2 (Kobayashi et al. 2004).

While there are very few studies investigating the importance of the p62-Nrf2-Keap1 pathway upon bacterial infection, a role for Nrf2 in regulating anti-oxidative stress responses has recently been demonstrated for viral infection (Olagnier et al. 2014). In accordance with our findings, the expression of Nrf2-dependent target genes limited ROS production during *Dengue virus* infection of dendritic cells, whereas genetic silencing of *Nrf2* enhanced ROS production and *Dengue*-induced cell death. Furthermore, genetic silencing of *Nrf2* increased IFN-β mRNA expression upon *Dengue virus* infection. In that particular study, however, the effect of IFN-β on regulating Nrf2-dependent redox homeostasis or cell death has not been addressed.

In one of the few studies investigating the role of the p62-Nrf2-Keap1 pathways during bacterial infection, Ichimura and colleagues reported that *S.* Typhimurium infection enhanced the expression of Nrf2-dependent cytoprotective genes in mouse embryonic fibroblasts (MEFs) (Ichimura et al. 2013). Apart from *Hmox-1*, however, we did not observe that *S.* Typhimurium infection induces a significant upregulation of anti-oxidant genes in WT macrophages. In our study, the transcription of Nrf2-dependent anti-oxidative genes is only enhanced in the absence of IFN-I signaling, indicating that IFN-I negatively regulates anti-oxidative stress responses. Another report from the same group suggested that *S.* Typhimurium activated the Keap1-Nrf2 system through phosphorylation of p62 at Ser351 during xenophagy (Ishimura et al. 2014). Accordingly, we found that *S.* Typhimurium infection induces p62 expression and interaction of p62 with Keap1 in macrophages. However, in the presence of IFN-I signaling the interaction of p62 with Keap1 is not sufficient to promote Nrf2-dependent cytoprotective responses. By contrast, loss of IFN-I signaling strongly enhances the interaction of p62 with Keap1 and increases Nrf2-dependent anti-oxidative stress responses to *S.* Typhimurium infection. Discrepancies to the results reported by Ishimura et al. could be attributed to the different cell types investigated, as the response to IFN-I during *S.* Typhimurium infection might differ in MEFs and BMDMs.

Similar to *Ifnar1*^{-/-} macrophages, we observed high p62 levels in autophagy-deficient *Atg7*^{-/-} macrophages after infection with *S*. Typhimurium. Despite p62 accumulation, however, autophagy deficiency does not result in enhanced macrophage survival. Accordingly, recent studies have demonstrated that autophagy defects sensitize cells to inflammatory cell death (Yonekawa and Thorburn 2013). Importantly, we found that blockade of IFN-I signaling significantly increases survival of *S*. Typhimurium-infected *Atg7*^{-/-} macrophages through the upregulation of Nrf2-dependent anti-oxidative genes.

Although our results suggest that p62 contributes to the regulation of Nrf2-dependent redox homeostasis and macrophage viability upon *S*. Typhimurium infection, we conclude that additional pathways besides p62 must be involved in regulating IFN-I-induced cell death.

4.5   *S*. Typhimurium infection activates Pgam5 downstream of IFN-I/RIP3

Previous studies have indicated that the expression of Nrf2-dependent genes was additionally regulated by the mitochondrial phosphatase Pgam5. Upon oxidative stress, Pgam5 was targeted to the outer membrane of mitochondria, where it formed a ternary complex with Nrf2 and Keap1. In this complex, dimeric Keap1 simultaneously bound both Pgam5 and Nrf2 (Lo and Hannink 2008). Importantly, knockdown of Pgam5 activated Nrf2-dependent ARE gene expression in Hela cells, indicating that Pgam5 is a negative regulator of antioxidant stress responses (Lo and Hannink 2008). In accordance with these findings, we demonstrate that Pgam5 is highly expressed in *S*. Typhimurium-infected macrophages and that Pgam5 negatively regulates Nrf2-dependent gene expression. Importantly, IFN-I signaling increases Pgam5 expression and enhances the interaction of Nrf2 with Pgam5 (presumably through Keap1) thereby impairing Nrf2 function.

Beyond regulating anti-oxidant stress responses, Pgam5 has also been reported to mediate RIP1/3-dependent necroptosis. Upon TNF receptor activation, Pgam5 formed a mitochondrial complex with RIP1- and RIP3 leading to Drp1-mediated mitochondrial fragmentation, a crucial step for necroptosis induction (Wang et al. 2012). Our present results indicate that during *S*. Typhimurium infection IFN-I activates RIP3, which induces expression

of Pgam5. In agreement with our observation that IFN-I signaling promotes Nrf2-Pgam5 complex formation, also the activation of the IFN-I downstream target RIP3 enhances the interaction of Nrf2 with Pgam5. Consequently, Pgam5 sequesters Nrf2 in the cytosol, which impairs the anti-oxidative stress response against *S*. Typhimurium.

4.6 *S.* Typhimurium infection induces cell death through impaired Nrf2 function

Over the last decades, considerable work has focused on *S*. Typhimurium-induced cell death of macrophages and multiple cell death pathways including caspase-1 and caspase-11-mediated pyroptosis (Man et al. 2017; Thurston et al. 2016) and RIP1/RIP3-mediated necroptosis (Robinson et al. 2012) have been identified. In our previous work we have demonstrated that IFN-I mediated the recruitment of RIP3 to the IFN-I receptor of *S*. Typhimurium-infected macrophages, which resulted in necroptosis execution (Robinson et al. 2012). Our present results indicate that IFN-I signaling impairs the ability of macrophages to respond to *S*. Typhimurium-induced oxidative stress by interfering with Nrf2 activation through decreased p62 and increased Pgam5 expression. The inability to respond to *S*. Typhimurium-induced damage finally results in macrophage death.

Our observation that pharmacological activation of Nrf2 protects macrophages from *S*. Typhimurium-induced cell death by limiting ROS production is in agreement with previous studies demonstrating an anti-oxidative, cytoprotective effect of Nrf2 enhancers (Liby et al. 2005; Yang et al. 2009). Importantly, we found that pharmacological activation of Nrf2 only prevents cell death of WT macrophages, whereas it has no additional effect in IFN-I deficient macrophages, where Nrf2 target genes are already highly upregulated. Consequently, we found that scavenging of mitochondrial ROS promotes macrophages survival after infection with *S*. Typhimurium.

Furthermore, our results demonstrate that IFN-I-regulated cell death is not a consequence of increased caspase-1 activation and subsequent pyroptosis, since IFN-I signaling reduces IL-1β secretion after *S*. Typhimurium infection. However, it remains to be investigated if caspase-11 is an additional player in IFN-I-regulated necroptosis in

S. Typhimurium-infected macrophages as IFN-I-induced GTPases are known to regulate caspase-11 activation (Meunier et al. 2014).

CONCLUSION

In conclusion, we have unraveled that the host´s IFN-I response exacerbates mitochondrial dysfunction upon *S.* Typhimurium infection of macrophages and that perturbed cellular redox homeostasis precedes *S.* Typhimurium-induced cell death. We propose a model, in which IFN-I/RIP3 signaling diminishes Nrf2-mediated anti-oxidative stress responses to *S.* Typhimurium infection through enhanced interaction of Nrf2 with Pgam5 (**Fig. 22**). The reduced ability to respond to *S.* Typhimurium-induced oxidative stress results in ROS-mediated mitochondrial damage, energy depletion and transient induction of autophagy. Autophagy post-transcriptionally downregulates p62 leading to perturbed p62-Keap1 interaction, which further represses Nrf2 function and eventually sensitizes macrophages to *S.* Typhimurium-induced necroptosis.

FUTURE PERSPECTIVES

Over the last decades, an alarming number of bacterial pathogens, particularly Gram-negative bacteria, has become resistant to standard antibiotic treatment. For some infections caused by multi-resistant bacteria even reserve antibiotics are no longer effective, which dramatically has increased morbidity and mortality rates. Host-directed therapies that modulate the patient´s immune response, rather than targeting the pathogen itself, could therefore be a novel treatment approach in the post-antibiotic era.

Our findings imply that inhibition of the host´s IFN-I signaling pathways could provide a therapeutic option for the supportive treatment of *S.* Typhimurium infection. Furthermore, we report here that increasing the Nrf2-dependent anti-oxidative response using pharmacological Nrf2 activators significantly improves infection outcome. Pharmacological interference with IFN-I signaling and Nrf2-dependent anti-oxidative responses might therefore be a novel treatment approach to combat Gram-negative infections in the future. Further studies are needed, however, to investigate whether our findings are transferable to infections caused by other Gram-negative or Gram-positive bacteria.

ACKNOWLEDGMENTS

BIBLIOGRAPHY

Aizawa SI. Bacterial flagella and type III secretion systems. FEMS Microbiol Lett. 2001; 202:157-164.

Arnoult D, Carneiro L, Tattoli I and Girardin SE. The role of mitochondria in cellular defense against microbial infection. Semin Immunol. 2009; 21:223-232.

Bakowski MA, Braun V and Brumell JH. Salmonella-containing vacuoles: directing traffic and nesting to grow. Traffic. 2008; 9:2022-2031.

Barber GN. STING: infection, inflammation and cancer. Nat Rev Immunol. 2015; 15:760-770.

Birmingham CL, Smith AC, Bakowski MA, Yoshimori T and Brumell JH. Autophagy controls Salmonella infection in response to damage to the Salmonella-containing vacuole. J Biol Chem. 2006; 281:11374-11383.

Bjorkoy G, Lamark T, Brech A, Outzen H, Perander M, Overvatn A, Stenmark H and Johansen T. p62/SQSTM1 forms protein aggregates degraded by autophagy and has a protective effect on huntingtin-induced cell death. J Cell Biol. 2005; 171:603-614.

Bogdan C, Mattner J and Schleicher U. The role of type I interferons in non-viral infections. Immunol Rev. 2004; 202:33-48.

Brennan MA and Cookson BT. Salmonella induces macrophage death by caspase-1-dependent necrosis. Mol Microbiol. 2000; 38:31-40.

Broz P, Ohlson MB and Monack DM. Innate immune response to Salmonella typhimurium, a model enteric pathogen. Gut Microbes. 2012; 3:62-70.

Cemma M and Brumell JH. Interactions of pathogenic bacteria with autophagy systems. Curr Biol. 2012; 22:R540-545.

Chandel NS. Mitochondria as signaling organelles. BMC Biol. 2014; 12:34.

Decker T, Muller M and Stockinger S. The yin and yang of type I interferon activity in bacterial infection. Nat Rev Immunol. 2005; 5:675-687.

Declercq W, Vanden Berghe T and Vandenabeele P. RIP kinases at the crossroads of cell death and survival. Cell. 2009; 138:229-232.

Denk H, Stumptner C, Fuchsbichler A, Muller T, Farr G, Muller W, Terracciano L and Zatloukal K. Are the Mallory bodies and intracellular hyaline bodies in neoplastic and non-neoplastic hepatocytes related? J Pathol. 2006; 208:653-661.

Deretic V, Saitoh T and Akira S. Autophagy in infection, inflammation and immunity. Nat Rev Immunol. 2013; 13:722-737.

Desvignes L, Wolf AJ and Ernst JD. Dynamic roles of type I and type II IFNs in early infection with Mycobacterium tuberculosis. J Immunol. 2012; 188:6205-6215.

Du Q, Xie J, Kim HJ and Ma X. Type I interferon: the mediator of bacterial infection-induced necroptosis. Cell Mol Immunol. 2013; 10:4-6.

Ejlerskov P, Hultberg JG, Wang J, Carlsson R, Ambjorn M, Kuss M, Liu Y, Porcu G, Kolkova K, Friis Rundsten C, Ruscher K, Pakkenberg B, Goldmann T, Loreth D, Prinz M, Rubinsztein DC and Issazadeh-Navikas S. Lack of Neuronal IFN-beta-IFNAR Causes Lewy Body- and Parkinson's Disease-like Dementia. Cell. 2015; 163:324-339.

Fitzwalter BE and Thorburn A. Recent insights into cell death and autophagy. FEBS J. 2015; 282:4279-4288.

Galluzzi L, Vitale I, Abrams JM, Alnemri ES, Baehrecke EH, Blagosklonny MV, Dawson TM, Dawson VL, El-Deiry WS, Fulda S, Gottlieb E, Green DR, Hengartner MO, Kepp O, Knight RA, Kumar S, Lipton SA, Lu X, Madeo F, Malorni W, Mehlen P, Nunez G, Peter ME, Piacentini M, Rubinsztein DC, Shi Y, Simon HU, Vandenabeele P, White E, Yuan J, Zhivotovsky B, Melino G and Kroemer G. Molecular definitions of cell death subroutines: recommendations of the Nomenclature Committee on Cell Death 2012. Cell Death Differ. 2012; 19:107-120.

Ganesan R, Hos NJ, Gutierrez S, Fischer J, Stepek JM, Daglidu E, Kronke M and Robinson N. Salmonella Typhimurium disrupts Sirt1/AMPK checkpoint control of mTOR to impair autophagy. PLoS Pathog. 2017; 13:e1006227.

Gough DJ, Messina NL, Clarke CJ, Johnstone RW and Levy DE. Constitutive type I interferon modulates homeostatic balance through tonic signaling. Immunity. 2012; 36:166-174.

Hara T, Nakamura K, Matsui M, Yamamoto A, Nakahara Y, Suzuki-Migishima R, Yokoyama M, Mishima K, Saito I, Okano H and Mizushima N. Suppression of basal autophagy in neural cells causes neurodegenerative disease in mice. Nature. 2006; 441:885-889.

Hensel M, Shea JE, Waterman SR, Mundy R, Nikolaus T, Banks G, Vazquez-Torres A, Gleeson C, Fang FC and Holden DW. Genes encoding putative effector proteins of the type III secretion system of Salmonella pathogenicity island 2 are required for bacterial virulence and proliferation in macrophages. Mol Microbiol. 1998; 30:163-174.

Hernandez LD, Pypaert M, Flavell RA and Galan JE. A Salmonella protein causes macrophage cell death by inducing autophagy. J Cell Biol. 2003; 163:1123-1131.

Hos NJ, Ganesan R, Gutierrez S, Hos D, Klimek J, Abdullah Z, Kronke M and Robinson N. Type I interferon enhances necroptosis of Salmonella Typhimurium-infected

macrophages by impairing antioxidative stress responses. J Cell Biol. 2017; 216:4107-4121.

Ichimura Y, Waguri S, Sou YS, Kageyama S, Hasegawa J, Ishimura R, Saito T, Yang Y, Kouno T, Fukutomi T, Hoshii T, Hirao A, Takagi K, Mizushima T, Motohashi H, Lee MS, Yoshimori T, Tanaka K, Yamamoto M and Komatsu M. Phosphorylation of p62 activates the Keap1-Nrf2 pathway during selective autophagy. Mol Cell. 2013; 51:618-631.

Inami Y, Waguri S, Sakamoto A, Kouno T, Nakada K, Hino O, Watanabe S, Ando J, Iwadate M, Yamamoto M, Lee MS, Tanaka K and Komatsu M. Persistent activation of Nrf2 through p62 in hepatocellular carcinoma cells. J Cell Biol. 2011; 193:275-284.

Ishii T, Itoh K and Yamamoto M. Roles of Nrf2 in activation of antioxidant enzyme genes via antioxidant responsive elements. Methods Enzymol. 2002; 348:182-190.

Ishimura R, Tanaka K and Komatsu M. Dissection of the role of p62/Sqstm1 in activation of Nrf2 during xenophagy. FEBS Lett. 2014; 588:822-828.

Itakura E and Mizushima N. p62 Targeting to the autophagosome formation site requires self-oligomerization but not LC3 binding. J Cell Biol. 2011; 192:17-27.

Jaramillo MC and Zhang DD. The emerging role of the Nrf2-Keap1 signaling pathway in cancer. Genes Dev. 2013; 27:2179-2191.

Jones BD, Ghori N and Falkow S. Salmonella typhimurium initiates murine infection by penetrating and destroying the specialized epithelial M cells of the Peyer's patches. J Exp Med. 1994; 180:15-23.

Kobayashi A, Kang MI, Okawa H, Ohtsuji M, Zenke Y, Chiba T, Igarashi K and Yamamoto M. Oxidative stress sensor Keap1 functions as an adaptor for Cul3-based E3 ligase to regulate proteasomal degradation of Nrf2. Mol Cell Biol. 2004; 24:7130-7139.

Komatsu M, Kurokawa H, Waguri S, Taguchi K, Kobayashi A, Ichimura Y, Sou YS, Ueno I, Sakamoto A, Tong KI, Kim M, Nishito Y, Iemura S, Natsume T, Ueno T, Kominami E, Motohashi H, Tanaka K and Yamamoto M. The selective autophagy substrate p62 activates the stress responsive transcription factor Nrf2 through inactivation of Keap1. Nat Cell Biol. 2010; 12:213-223.

Komatsu M, Waguri S, Chiba T, Murata S, Iwata J, Tanida I, Ueno T, Koike M, Uchiyama Y, Kominami E and Tanaka K. Loss of autophagy in the central nervous system causes neurodegeneration in mice. Nature. 2006; 441:880-884.

Komatsu M, Waguri S, Koike M, Sou YS, Ueno T, Hara T, Mizushima N, Iwata J, Ezaki J, Murata S, Hamazaki J, Nishito Y, Iemura S, Natsume T, Yanagawa T, Uwayama J, Warabi E, Yoshida H, Ishii T, Kobayashi A, Yamamoto M, Yue Z, Uchiyama Y,

Kominami E and Tanaka K. Homeostatic levels of p62 control cytoplasmic inclusion body formation in autophagy-deficient mice. Cell. 2007; 131:1149-1163.

Kroemer G, Galluzzi L and Brenner C. Mitochondrial membrane permeabilization in cell death. Physiol Rev. 2007; 87:99-163.

Lambeth JD. NOX enzymes and the biology of reactive oxygen. Nat Rev Immunol. 2004; 4:181-189.

Lan R, Reeves PR and Octavia S. Population structure, origins and evolution of major Salmonella enterica clones. Infect Genet Evol. 2009; 9:996-1005.

LaRock DL, Chaudhary A and Miller SI. Salmonellae interactions with host processes. Nat Rev Microbiol. 2015; 13:191-205.

Lau A, Wang XJ, Zhao F, Villeneuve NF, Wu T, Jiang T, Sun Z, White E and Zhang DD. A noncanonical mechanism of Nrf2 activation by autophagy deficiency: direct interaction between Keap1 and p62. Mol Cell Biol. 2010; 30:3275-3285.

Levine B, Mizushima N and Virgin HW. Autophagy in immunity and inflammation. Nature. 2011; 469:323-335.

Lewis JA, Huq A and Najarro P. Inhibition of mitochondrial function by interferon. J Biol Chem. 1996; 271:13184-13190.

Li T and Chen ZJ. The cGAS-cGAMP-STING pathway connects DNA damage to inflammation, senescence, and cancer. J Exp Med. 2018; 215:1287-1299.

Liby K, Hock T, Yore MM, Suh N, Place AE, Risingsong R, Williams CR, Royce DB, Honda T, Honda Y, Gribble GW, Hill-Kapturczak N, Agarwal A and Sporn MB. The synthetic triterpenoids, CDDO and CDDO-imidazolide, are potent inducers of heme oxygenase-1 and Nrf2/ARE signaling. Cancer Res. 2005; 65:4789-4798.

Lindgren SW, Stojiljkovic I and Heffron F. Macrophage killing is an essential virulence mechanism of Salmonella typhimurium. Proc Natl Acad Sci U S A. 1996; 93:4197-4201.

Lo SC and Hannink M. PGAM5, a Bcl-XL-interacting protein, is a novel substrate for the redox-regulated Keap1-dependent ubiquitin ligase complex. J Biol Chem. 2006; 281:37893-37903.

Lo SC and Hannink M. PGAM5 tethers a ternary complex containing Keap1 and Nrf2 to mitochondria. Exp Cell Res. 2008; 314:1789-1803.

Majowicz SE, Musto J, Scallan E, Angulo FJ, Kirk M, O'Brien SJ, Jones TF, Fazil A, Hoekstra RM and International Collaboration on Enteric Disease 'Burden of Illness S. The global burden of nontyphoidal Salmonella gastroenteritis. Clin Infect Dis. 2010; 50:882-889.

Man SM, Karki R, Briard B, Burton A, Gingras S, Pelletier S and Kanneganti TD. Differential roles of caspase-1 and caspase-11 in infection and inflammation. Sci Rep. 2017; 7:45126.

Marinho FV, Benmerzoug S, Oliveira SC, Ryffel B and Quesniaux VFJ. The Emerging Roles of STING in Bacterial Infections. Trends Microbiol. 2017; 25:906-918.

Mathew R, Karp CM, Beaudoin B, Vuong N, Chen G, Chen HY, Bray K, Reddy A, Bhanot G, Gelinas C, Dipaola RS, Karantza-Wadsworth V and White E. Autophagy suppresses tumorigenesis through elimination of p62. Cell. 2009; 137:1062-1075.

Medzhitov R. Toll-like receptors and innate immunity. Nat Rev Immunol. 2001; 1:135-145.

Meunier E, Dick MS, Dreier RF, Schurmann N, Kenzelmann Broz D, Warming S, Roose-Girma M, Bumann D, Kayagaki N, Takeda K, Yamamoto M and Broz P. Caspase-11 activation requires lysis of pathogen-containing vacuoles by IFN-induced GTPases. Nature. 2014; 509:366-370.

Mihaylova MM and Shaw RJ. The AMPK signalling pathway coordinates cell growth, autophagy and metabolism. Nat Cell Biol. 2011; 13:1016-1023.

Mizushima N, Levine B, Cuervo AM and Klionsky DJ. Autophagy fights disease through cellular self-digestion. Nature. 2008; 451:1069-1075.

Murphy MP. How mitochondria produce reactive oxygen species. Biochem J. 2009; 417:1-13.

O'Connell RM, Saha SK, Vaidya SA, Bruhn KW, Miranda GA, Zarnegar B, Perry AK, Nguyen BO, Lane TF, Taniguchi T, Miller JF and Cheng G. Type I interferon production enhances susceptibility to Listeria monocytogenes infection. J Exp Med. 2004; 200:437-445.

Olagnier D, Peri S, Steel C, van Montfoort N, Chiang C, Beljanski V, Slifker M, He Z, Nichols CN, Lin R, Balachandran S and Hiscott J. Cellular oxidative stress response controls the antiviral and apoptotic programs in dengue virus-infected dendritic cells. PLoS Pathog. 2014; 10:e1004566.

Owen KA, Anderson CJ and Casanova JE. Salmonella Suppresses the TRIF-Dependent Type I Interferon Response in Macrophages. MBio. 2016; 7:e02051-02015.

Owen KA, Meyer CB, Bouton AH and Casanova JE. Activation of focal adhesion kinase by Salmonella suppresses autophagy via an Akt/mTOR signaling pathway and promotes bacterial survival in macrophages. PLoS Pathog. 2014; 10:e1004159.

Pankiv S, Clausen TH, Lamark T, Brech A, Bruun JA, Outzen H, Overvatn A, Bjorkoy G and Johansen T. p62/SQSTM1 binds directly to Atg8/LC3 to facilitate degradation of ubiquitinated protein aggregates by autophagy. J Biol Chem. 2007; 282:24131-24145.

Pasparakis M and Vandenabeele P. Necroptosis and its role in inflammation. Nature. 2015; 517:311-320.

Platanias LC. Mechanisms of type-I- and type-II-interferon-mediated signalling. Nat Rev Immunol. 2005; 5:375-386.

Robert Koch Institute. www.rki.de/DE/Content/Infekt/EpidBull/Merkblaetter/-Ratgeber_Salmonellose.html. 2019.

Robinson N, McComb S, Mulligan R, Dudani R, Krishnan L and Sad S. Type I interferon induces necroptosis in macrophages during infection with Salmonella enterica serovar Typhimurium. Nat Immunol. 2012; 13:954-962.

Rubinsztein DC. The roles of intracellular protein-degradation pathways in neurodegeneration. Nature. 2006; 443:780-786.

Rushmore TH, Morton MR and Pickett CB. The antioxidant responsive element. Activation by oxidative stress and identification of the DNA consensus sequence required for functional activity. J Biol Chem. 1991; 266:11632-11639.

Ryan KJ and Ray CG. Sherris Medical Microbiology: An Introduction to Infectious Disease. (Fourth Edition). 2004.

Schmeisser H, Fey SB, Horowitz J, Fischer ER, Balinsky CA, Miyake K, Bekisz J, Snow AL and Zoon KC. Type I interferons induce autophagy in certain human cancer cell lines. Autophagy. 2013; 9:683-696.

Shi CS and Kehrl JH. MyD88 and Trif target Beclin 1 to trigger autophagy in macrophages. J Biol Chem. 2008; 283:33175-33182.

Sing A, Merlin T, Knopf HP, Nielsen PJ, Loppnow H, Galanos C and Freudenberg MA. Bacterial induction of beta interferon in mice is a function of the lipopolysaccharide component. Infect Immun. 2000; 68:1600-1607.

Stark GR and Darnell JE, Jr. The JAK-STAT pathway at twenty. Immunity. 2012; 36:503-514.

Stavru F, Bouillaud F, Sartori A, Ricquier D and Cossart P. Listeria monocytogenes transiently alters mitochondrial dynamics during infection. Proc Natl Acad Sci U S A. 2011; 108:3612-3617.

Stumptner C, Fuchsbichler A, Zatloukal K and Denk H. In vitro production of Mallory bodies and intracellular hyaline bodies: the central role of sequestosome 1/p62. Hepatology. 2007; 46:851-860.

Sumpter R, Jr. and Levine B. Autophagy and innate immunity: triggering, targeting and tuning. Semin Cell Dev Biol. 2010; 21:699-711.

Thompson HG, Harris JW, Wold BJ, Lin F and Brody JP. p62 overexpression in breast tumors and regulation by prostate-derived Ets factor in breast cancer cells. Oncogene. 2003; 22:2322-2333.

Thurston TL, Matthews SA, Jennings E, Alix E, Shao F, Shenoy AR, Birrell MA and Holden DW. Growth inhibition of cytosolic Salmonella by caspase-1 and caspase-11 precedes host cell death. Nat Commun. 2016; 7:13292.

Thurston TL, Ryzhakov G, Bloor S, von Muhlinen N and Randow F. The TBK1 adaptor and autophagy receptor NDP52 restricts the proliferation of ubiquitin-coated bacteria. Nat Immunol. 2009; 10:1215-1221.

Tindall BJ, Grimont PA, Garrity GM and Euzeby JP. Nomenclature and taxonomy of the genus Salmonella. Int J Syst Evol Microbiol. 2005; 55:521-524.

Travassos LH, Carneiro LA, Ramjeet M, Hussey S, Kim YG, Magalhaes JG, Yuan L, Soares F, Chea E, Le Bourhis L, Boneca IG, Allaoui A, Jones NL, Nunez G, Girardin SE and Philpott DJ. Nod1 and Nod2 direct autophagy by recruiting ATG16L1 to the plasma membrane at the site of bacterial entry. Nat Immunol. 2010; 11:55-62.

Umemura A, He F, Taniguchi K, Nakagawa H, Yamachika S, Font-Burgada J, Zhong Z, Subramaniam S, Raghunandan S, Duran A, Linares JF, Reina-Campos M, Umemura S, Valasek MA, Seki E, Yamaguchi K, Koike K, Itoh Y, Diaz-Meco MT, Moscat J and Karin M. p62, Upregulated during Preneoplasia, Induces Hepatocellular Carcinogenesis by Maintaining Survival of Stressed HCC-Initiating Cells. Cancer Cell. 2016; 29:935-948.

Vanden Berghe T, Linkermann A, Jouan-Lanhouet S, Walczak H and Vandenabeele P. Regulated necrosis: the expanding network of non-apoptotic cell death pathways. Nat Rev Mol Cell Biol. 2014; 15:135-147.

Vanlangenakker N, Vanden Berghe T, Krysko DV, Festjens N and Vandenabeele P. Molecular mechanisms and pathophysiology of necrotic cell death. Curr Mol Med. 2008; 8:207-220.

Vazquez-Torres A, Jones-Carson J, Baumler AJ, Falkow S, Valdivia R, Brown W, Le M, Berggren R, Parks WT and Fang FC. Extraintestinal dissemination of Salmonella by CD18-expressing phagocytes. Nature. 1999; 401:804-808.

Wang Z, Jiang H, Chen S, Du F and Wang X. The mitochondrial phosphatase PGAM5 functions at the convergence point of multiple necrotic death pathways. Cell. 2012; 148:228-243.

Wasilewski M and Scorrano L. The changing shape of mitochondrial apoptosis. Trends Endocrinol Metab. 2009; 20:287-294.

Wasserman WW and Fahl WE. Functional antioxidant responsive elements. Proc Natl Acad Sci U S A. 1997; 94:5361-5366.

Weinberg SE, Sena LA and Chandel NS. Mitochondria in the regulation of innate and adaptive immunity. Immunity. 2015; 42:406-417.

West AP, Brodsky IE, Rahner C, Woo DK, Erdjument-Bromage H, Tempst P, Walsh MC, Choi Y, Shadel GS and Ghosh S. TLR signalling augments macrophage bactericidal activity through mitochondrial ROS. Nature. 2011; 472:476-480.

World Health Organisation. www.who.int/news-room/fact-sheets/detail/salmonella-(non-typhoidal). 2019.

Yamamoto M, Sato S, Hemmi H, Uematsu S, Hoshino K, Kaisho T, Takeuchi O, Takeda K and Akira S. TRAM is specifically involved in the Toll-like receptor 4-mediated MyD88-independent signaling pathway. Nat Immunol. 2003; 4:1144-1150.

Yang L, Calingasan NY, Thomas B, Chaturvedi RK, Kiaei M, Wille EJ, Liby KT, Williams C, Royce D, Risingsong R, Musiek ES, Morrow JD, Sporn M and Beal MF. Neuroprotective effects of the triterpenoid, CDDO methyl amide, a potent inducer of Nrf2-mediated transcription. PLoS One. 2009; 4:e5757.

Yonekawa T and Thorburn A. Autophagy and cell death. Essays Biochem. 2013; 55:105-117.

Zatloukal K, Stumptner C, Fuchsbichler A, Heid H, Schnoelzer M, Kenner L, Kleinert R, Prinz M, Aguzzi A and Denk H. p62 Is a common component of cytoplasmic inclusions in protein aggregation diseases. Am J Pathol. 2002; 160:255-263.

Zhang DD, Lo SC, Cross JV, Templeton DJ and Hannink M. Keap1 is a redox-regulated substrate adaptor protein for a Cul3-dependent ubiquitin ligase complex. Mol Cell Biol. 2004; 24:10941-10953.

Zheng YT, Shahnazari S, Brech A, Lamark T, Johansen T and Brumell JH. The adaptor protein p62/SQSTM1 targets invading bacteria to the autophagy pathway. J Immunol. 2009; 183:5909-5916.

Zhong Z, Umemura A, Sanchez-Lopez E, Liang S, Shalapour S, Wong J, He F, Boassa D, Perkins G, Ali SR, McGeough MD, Ellisman MH, Seki E, Gustafsson AB, Hoffman HM, Diaz-Meco MT, Moscat J and Karin M. NF-kappaB Restricts Inflammasome Activation via Elimination of Damaged Mitochondria. Cell. 2016; 164:896-910.

Zorov DB, Juhaszova M and Sollott SJ. Mitochondrial reactive oxygen species (ROS) and ROS-induced ROS release. Physiol Rev. 2014; 94:909-950.

DECLARATION

„Ich versichere, dass ich die von mir vorgelegte Dissertation selbstständig angefertigt, die benutzten Quellen und Hilfsmittel vollständig angegeben und die Stellen der Arbeit - einschließlich Tabellen, Karten und Abbildungen -, die anderen Werken im Wortlaut oder dem Sinn nach entnommen sind, in jedem Einzelfall als Entlehnung kenntlich gemacht habe; dass diese Dissertation noch keiner anderen Fakultät oder Universität zur Prüfung vorgelegen hat; dass sie - abgesehen von unten angegebenen Teilpublikationen - noch nicht veröffentlicht worden ist sowie, dass ich eine solche Veröffentlichung vor Abschluss des Promotionsverfahrens nicht vornehmen werde. Die Bestimmungen dieser Promotionsordnung sind mir bekannt. Die von mir vorgelegte Dissertation ist von Prof. Martin Krönke und Dr. Nirmal Robinson betreut worden."

Übersicht der Publikationen:

Hos NJ, Ganesan R, Gutierrez S, Hos D, Klimek J, Abdullah Z, Krönke M, Robinson N. Type I interferon enhances necroptosis of Salmonella Typhimurium-infected macrophages by impairing anti-oxidative stress responses. *The Journal of Cell Biology* (2017). 216(12):4107-4121. doi: 10.1083/jcb.201701107

Ganesan R, **Hos NJ**, Gutierrez S, Fischer J, Stepek JM, Daglidu E, Krönke M, Robinson N. *Salmonella* Typhimurium disrupts Sirt1/AMPK checkpoint control of mTOR to impair autophagy. *PLoS Pathogens* (2017). 13;13(2):e1006227. doi: 10.1371/journal.ppat.1006227

„Ich versichere, dass ich alle Angaben wahrheitsgemäß nach bestem Wissen und Gewissen gemacht habe und verpflichte mich, jedmögliche, die obigen Angaben betreffen-den Veränderungen, dem Promotionsausschuss unverzüglich mitzuteilen."

Köln, 14.06.2019